National Technical University of Ukraine
"Ihor Sikorsky Kyiv Polytechnic Institute"
Educational and Scientific Institute of Aerospace Technologies
Department of Aircraft and Rocket Engineering

Admitted to the defense
Performing duties of the Department head

_____ Oleksandr BONDARENKO
" " _____ 2023

Degree project
to obtain a bachelor's degree
under the educational and professional program "Airplanes and Helicopters"
specialty 134 "Aviation and rocket-space engineering"
on the topic: " «A mid-range jet reconnaissance drone»"

Performed by:
student of the 4th year, group AL-94
Bahattin Yiğit Kademlioğlu _____

Supervisor :
Associate Professor, Ph.D.
Oleksandr Mykolayovych Bondarenko _____

Recenser:
Senior teacher, Ph.D.,
Oleksiy Viktorovich Sholohov _____

I certify that in this diploma project there are no borrowings from the works of other authors without appropriate references.
Student _____

Kyiv – 2023

National Technical University of Ukraine

“Igor Sikorsky Kyiv Polytechnic Institute”

Education and Research Institute of Aerospace Technologies

Department of Aircraft and Aeronautical Engineering

Level of higher education - first (bachelor's)

Specialty – 134 "Aviation and Aeronautical and space technology"
Educational and professional program "Airplanes and helicopters"

APPROVED
Performing duties of the Department head
_____ Oleksandr BONDARENKO
(signature) (initials, last name)
«____» _____ 2023 year

TASK
for the diploma project of the student
Bahattin Yiğit Kademlioğlu
(surname, first name, patronymic, academic degree, academic title)

1. . Project topic «A mid-range jet reconnaissance drone», Project supervisor Oleksandr BONDARENKO, p.h.d., approved by the university order dated 31.05. 2023 p. №2085-c

2. Deadline for submitting project by student *16.06.2023 p.*

3. Initial data for project:_____

3.1 Flight height H=0...12000m.
3.2. Cruising speed V = 1000 km/h
3.3. . Flight weight no more than m = 3500 kg.
3.4. Payload – 600 kg
3.5. Flight duration t = 5 hour
3.6. Flight distance – 4000 km
3.7. Type of engines – turbo jet.

4. Content of the settlement and explanatory note: _____

4.1. The state of problem and directions for their solution..
4.2 . General layout of the UAV.
4.3. Modeling.
4.4. Calculation of base characteristics.
4.5. Development of design.
4.6 Development of making technology

5. List of graphic (illustrative) material (indicating mandatory drafters, posters, presentations, etc.)

5.1 Overview of analogues.

5.2 Calculation results

5.3 Design of the drone (all view drawing).

5.4. Making technology

6. Projecr parts consultant

Part	Name of consultant	Signature, Date	
		task issued	task accepted

7. Date of issue of the assignment: ___*1. 02. 2023*_____

CALENDAR PLAN

№ з/п	The stage titles of the diploma project completion	The fulfillment term of project stages	Note
1.	*Selection and analysis of literature*	until 15.03.2021	
2.	*Analysis of the design methodology*	until *25.03.2022 p.*	
3.	*Solid state modeling*	until *10.04.2022 p.*	
4.	*Optimization of design*	until *20.04.2022 p.*	
5.	*Calculation of base characteristics*	until *5.05.2022 p.*	
6.	*Design*	until *15.05.2022 p.*	
7.	Development of manufacturing technology	until *24.05.2022 p.*	
8.	*Registration of an explanatory note and graphic materials*	until *27.05.2022 p.*	
9.	*Designing an explanatory note and graphic materials. Supervisor answears.*	until *06.06.2022 p.*	
10.	Check for plagiarism	until *10.06.2022 p.*	
11.	*Recensing of*	until *12.06.2022 p.*	
12.	*Defence*	*from 14.06.2022 p. to 17.06.2022 p*	

Student _____ Bahattin Yiğit Kademlioğlu

Project supervisor _____ Oleksandr BONDARENKO

DIPLOMA PROJECT INFORMATION

№ p.p.	Format	Designation	Name	Quantity sheets	A note
1	A4		TASK for the diploma project	2	
2	A4	АЛ9412.06.00.00.00 EN	Explanatory note	61	
3	A1	АЛ9412.06.00.00.00All	Design of the drone (all view drawing)	1	
4	A1	АЛ9412.06.00.00.01	Overview of analogues	1	
5	A1	АЛ9412.06.00.00.02	Calculation results	1	
5	A1	АЛ9412.06.00.00.03	Making technology	1	

				АЛ9412.06.00.0000	
	last name, initials	Sign.	Date		
Performed	Kademlioğlu I.B..			Sheet	Sheets
Checked	Bondarenko O.M.			4	63
				Igor Sikorsky Kyiv Polytechnic Institute	
N.contr.	Povarov S.A.				
Dep. head	Bondarenko O.M.				

Diploma project information

Explanatory note
to the diploma project

on the topic: "A mid-range jet reconnaissance drone "

Kyiv - 2023

Abstract

The thesis contains: 67 pages, 42 figures, 3 tables, 12 used sources, 0 appendices.

The acquisition of practical skills in the development of structures, the analysis of aggregate structures and the justified choice of the most appropriate structures are among the most important tasks facing students in the process of education.

The goal of the individual thesis task is to increase the aerodynamic characteristics of an unmanned aerial vehicle due to increasing the flight range and increasing the resources of an unmanned aerial vehicle wing.

During the performance of the pre-diploma work, an analysis of modern scientific and technical literature was carried out , a search and analysis of medical five-seater aircraft , comparative characteristics of aerodynamic, technical and flight characteristics of three modern light jet aircraft. On the basis of the conducted analysis , a choice was made optimal models for serving work and selected optimal in model _ aerodynamic profile unmanned the plane average class _

The conducted research makes it possible to carry out further development of the calculation model of an unmanned unmanned aircraft of the middle class, the calculation of the resource, range and duration of the flight.

CONTENT

LIST OF CONVENTIONAL ABBREVIATIONS

					АЛ9412.06.00.0000 EN			
Ch.	Sheet	N document	Sign.	Date	A mid-range jet reconnaissance drone	Let.	Mass	Scale
Performed		*Kademlioğlu*						
Checked		*Bondarenko*				Sheet 7	Sheets 66	
T.Contr.								
Reviewer								
N.contr		*Povarov*				NN IAT, Igor Sikorsky Kyiv Polytechnicl Institute		
Approved		*Bondarenko*						

LIST OF CONVENTIONAL ABBREVIATIONS

UAV - unmanned aerial vehicle

SGS - second, gram, centimeter.

TK - technical task.

CM - composite materials

DB - database;

GM - geometric model;

FE - finite element;

FEM - finite element method;

BPC - the broken part of the caisson (wings);

PZ - software;

PSL - plane of symmetry of the plane;

CAD - system of computer aid design

CFRP - Carbon Fibre Reinforced Polymer

1. SELECTION AND ANALYSIS OF LITERATURE

Tu-141 "Stryzh" is a reusable Soviet operational -tactical reconnaissance unmanned aerial vehicle developed by the DKB named after A.N. Tupolev, was part of the BP-2 "Stryzh" complex (fig.1).

Fig.1. Oll view of UAV Tu-141 "Stryzh" on start platform

Tu-141 had an all-metal, low-wing glider , made according to the " tailless " scheme of PGO. A triangular wing with a leading edge sweep of 58°, had small inflows in the root parts. PGO — can be adjusted on the ground in the range from 0° to 8° depending on the centering of the unmanned aircraft, trapezoidal in plan, with a yaw angle along the leading edge of 41.3°. Vertical feathering was carried out with a sweep along the leading edge of 52°. Control of the aircraft was carried out with the help of two-section elevons on the wing and a direct rudder. The fuselage has a round shape with a diameter in the cylindrical part of 950 mm, which Ch.s to an oval one in the area of the engine installation. The TRD air intake above the fuselage is subsonic, installed above the fuselage. On the aircraft "141" was installed TRD type R9A-300 or KR-17A on machines of late releases, with a static thrust of 2000 kgf . The engine was

arranged at an angle of 4.5° to the axis of the unmanned aircraft. Maximum speed: 1000 km/h.

It was intended for reconnaissance at a depth of up to 400 kilometers from the front line at transonic speeds. It was equipped with means of photo and infrared reconnaissance, which allowed it to be used under any conditions and at any time of the day. The landing of the Tu-141 unmanned aircraft was carried out using a parachute system located in the tail part.

One of first jet aircraft is made of steel and aluminum alloys with extensive use of welding (fig.2).

Fig.2. Oll view of typical jet aircraft

The wing consoles have a trapezoidal shape in plan and can be set at a sweep angle of 16, 45 and 72 along the leading edge. Each console has slats, four-section flaps and two-section interceptors. Equipped with a turbojet two-circuit engine with afterburner chambers. Maximum speed near the ground: 1350 km/h. Maximum speed at altitude: 2500 km/h.

Bayraktar MIUS is a jet subsonic stealthy deck-based UAV developed by the Turkish company Baykar Makina (fig.3). The UAV has a maximum take-off weight of more than 5.5 tons , of which more than 1,500 kg is its payload, equipped with one turboprop engine. While the MIUS-A will be near supersonic

with the Ukrainian AI-25TLT engine, the MIUS-B will be supersonic with the Ukrainian AI-322F engine and the Turkish TEI TF-6000.

Fig. 3. Jet subsonic stealthy deck-based UAV

MIUS-B will have a 2.5 times more powerful engine, which significantly distinguishes it from MIUS-A in terms of technical characteristics. It is assumed that MIUS will be launched from TCG Anadolu (L-400) without the help of a catapult system. Vertical tail and front horizontal rudders ("duck" aerodynamic scheme). Developed using stealth technology and has a small effective scattering area (EPR). Maximum speed: 900 km/h.

Bayraktar was chosen as the prototype for this work Kizilelma .

Analysis of scientific and technical literature on the construction of aircraft allowed to choose the promising Bayraktar UAV project as a prototype Kuzilelma with an aerodynamic "duck" design.

The advantage of this scheme is the provision of pitch control without loss of lifting force for balancing, since the lifting force of the PGO coincides in direction with the lifting force of the main wing, in contrast to the normal aerodynamic scheme, in which the rear horizontal tail creates a negative lifting force. Aircraft of this scheme also have greater maneuverability compared to the

normal scheme. This scheme protects the aircraft from stalling in a corkscrew - the air flow on the PGO occurs earlier than on the wing, which creates most of the lifting force, so the nose of the unmanned aircraft in this case is slightly lowered, and the machine returns to normal flight.

Component diagram and characteristics an all-rotating front horizontal tail (PGO) was chosen . There are two options for choosing a scheme for the wing:

1) Sagittal wing
2) Inverted sweep wing

Providing the wing with a certain sweep is the most effective means of increasing the critical number M of flight $_{crit}$. Increasing the sweep of the wing not only delays the onset of the wave crisis at higher speeds, but also smoothes its flow and significantly reduces the increase in drag. In addition, the sagittality of the wing directly increases the critical speed of flutter and divergence.

On the other hand, the sweep causes a decrease in the carrying capacity of the wing - a decrease in the coefficient of lifting force $C_{in\ max}$, the aerodynamic quality of the wing K_{max} , and the effectiveness of the mechanization of the wing also deteriorates. Due to the phenomenon of lateral flow of the boundary layer to the ends of the swept wing, there is a tendency for the flow to end at high angles of attack, which leads to the loss of lateral controllability and subsequent instability of the unmanned aircraft in the transverse channel.

Having analyzed the scientific and technical literature, we can say that the wing with inverted sweep is partially free from this drawback. First, the reverse swept wing has no terminal stalls and therefore has higher lift. Secondly, the disruption of the flow at large angles of attack in such a wing occurs first at its root part, without disrupting the operation of the ailerons, leaving the aircraft controllable.

Tests of the Kh-29 (fig.4) Grumman unmanned aircraft showed that the inverted sweep wing provides: some improvement in aerodynamic quality during maneuvering, especially at low speeds; greater lifting force compared to

a wing with a straight sweep , and therefore a greater relative load capacity; better controllability at low subsonic speeds (and, as a result, improved take-off and landing characteristics); lower speed of piling into a corkscrew.

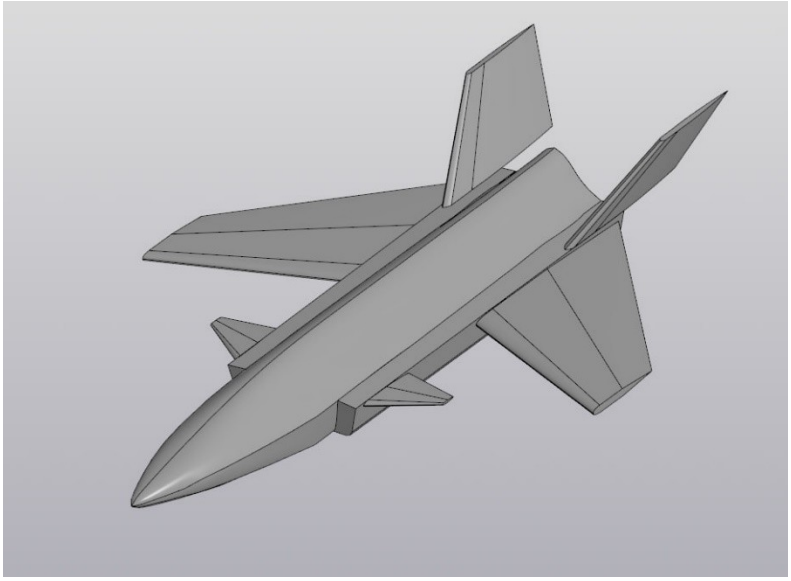

Fig. 4. Inverted sweep wing

The tail feathers are double-keeled .

Air intakes are symmetrical on the sides relative to the longitudinal axis of symmetry.

Flight range – 1000+ km.

The flight speed is transonic /supersonic (980-1470 km/h).

1. Design tasks:
    - Construction
    - Choose optimal aerodynamic shapes
    - Modes of operation of the complex
2. Optimization of aerodynamic characteristics

Conclusion to the chapter

The analysis of modern scientific and technical literature was carried out , the technical and flight characteristics of two modern light jet unmanned aircraft were considered. Designs were considered, and a prototype was selected for further work on the development of our own light five- seater glider unmanned aircraft. On the basis of the conducted analysis , a choice was made optimal models for serving work and selected optimal in model aerodynamic profile unmanned the plane average class.

2. Development of the design of the glider

Creo program was used to create models of spar belts Parametric .
The spar should consist of two belts of a standard rolled profile for the length of the track of the transverse power set and a wall made of sheet material. The spar will lie in one plane of symmetry to ensure manufacturability of assembly.

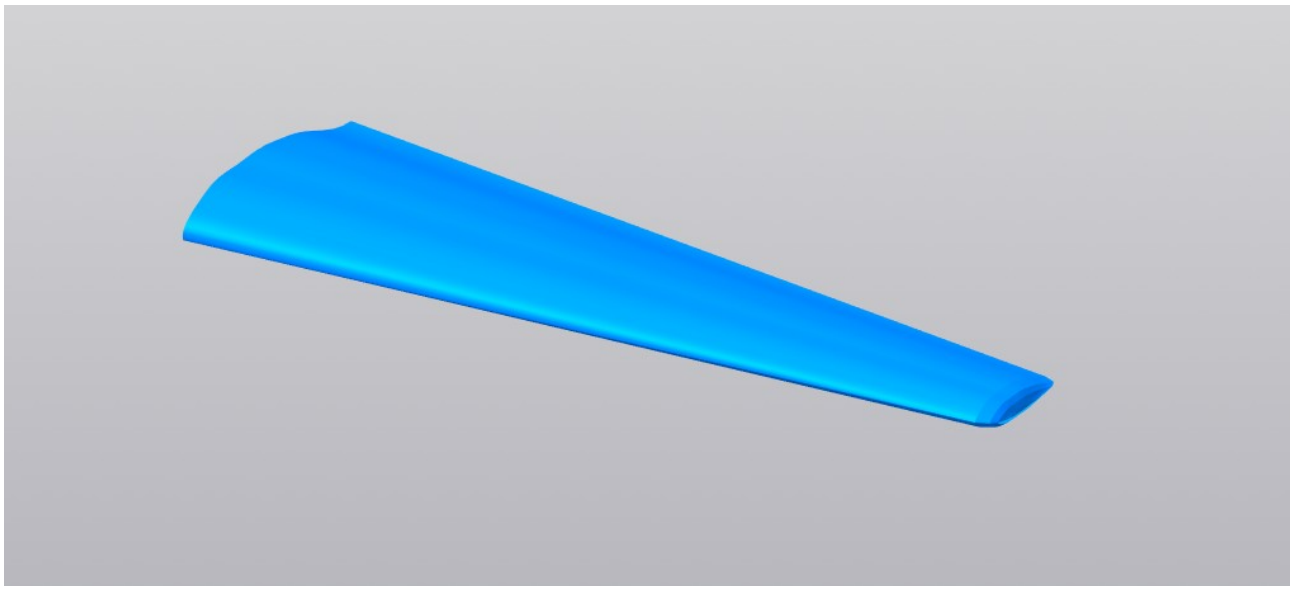

Fig. 5. Constructed wing profile

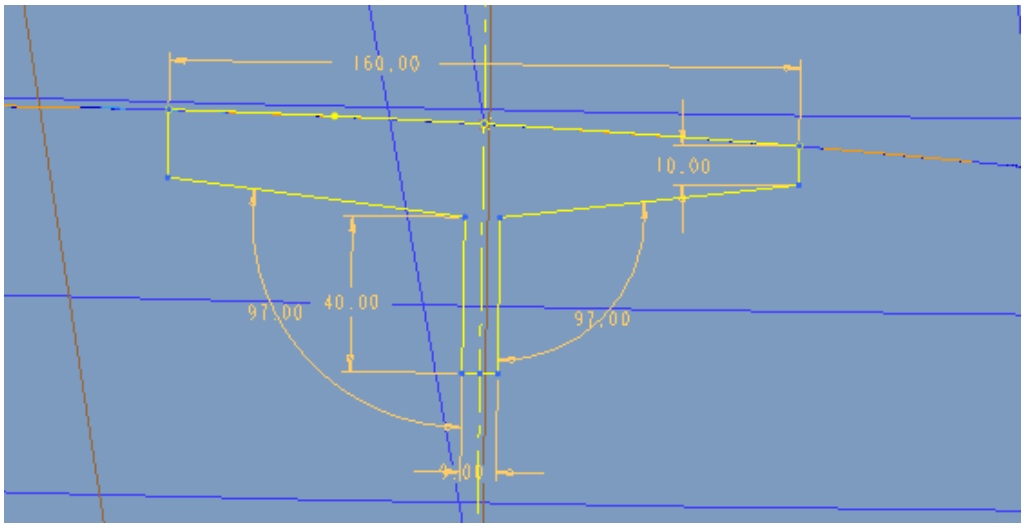

Fig. 6. Section of the upper belt of the spar in the final profile

					АЛ9412.06.00.00.00EN	Sheet
Ch.	Sheet	N document	Sign.	Date		

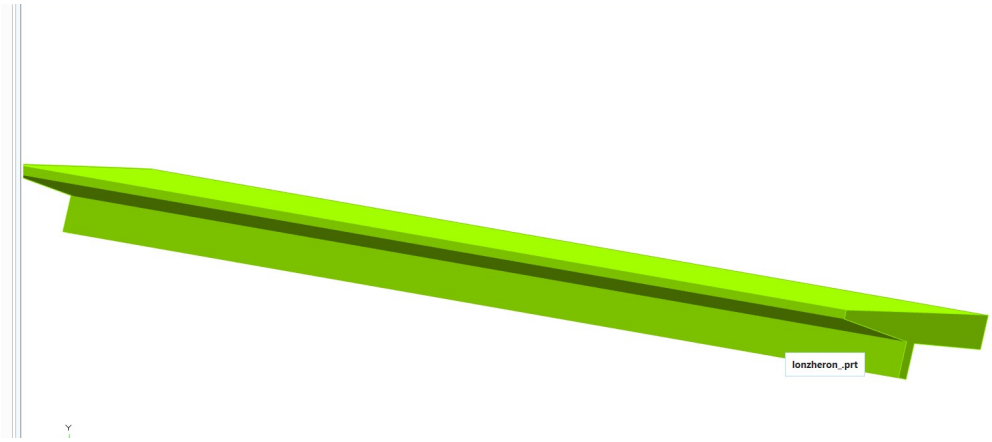

Fig. 7. Upper spar

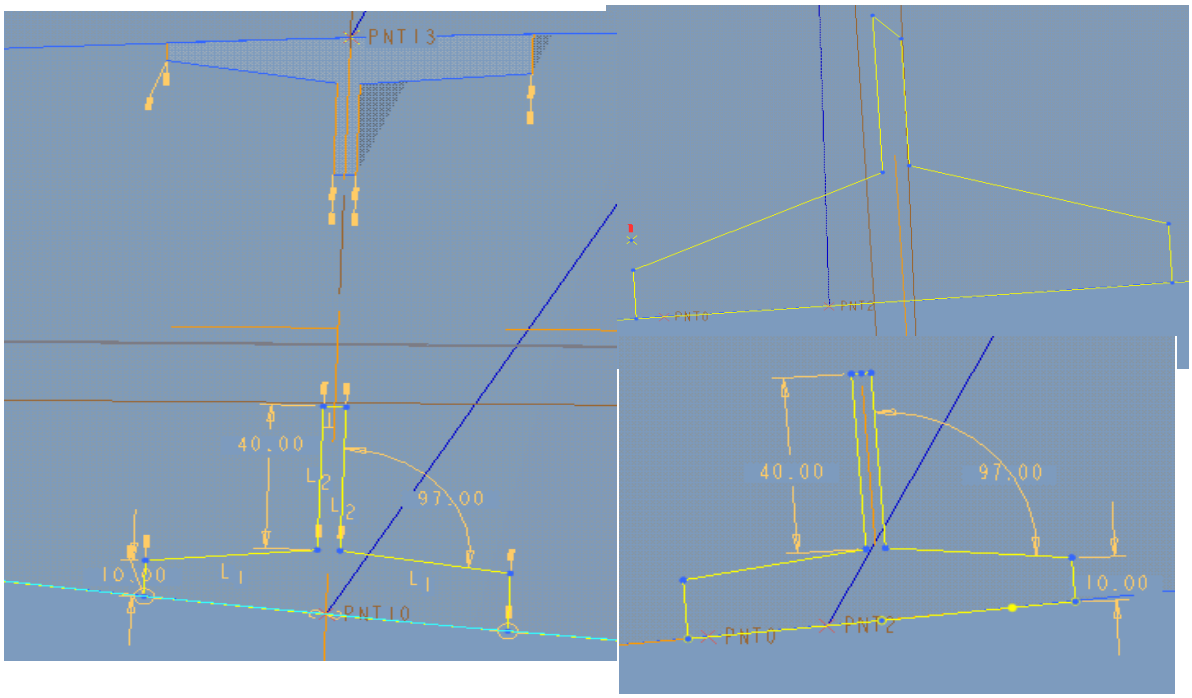

Fig. 8. Construction of sketches of the lower belt of the spar

Fig. 9. Lower spar

					АЛ9412.06.00.00.00EN	Sheet
Ch.	Sheet	N document	Sign.	Date		

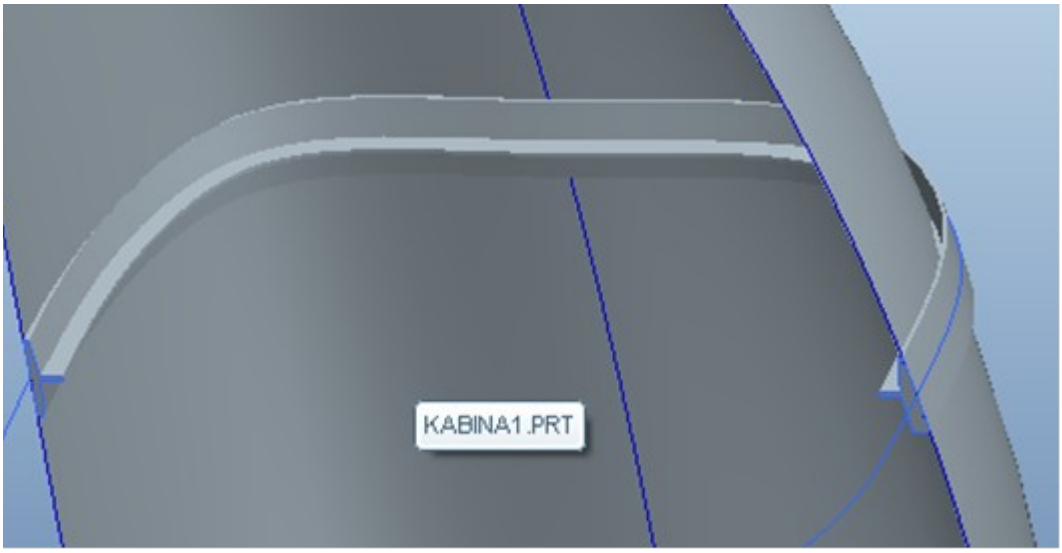

Fig. 10. Construction of the fuselage frame

The following steps in the construction of the airframe were performed using the CAD system Compass - 3D _ v 18.1.

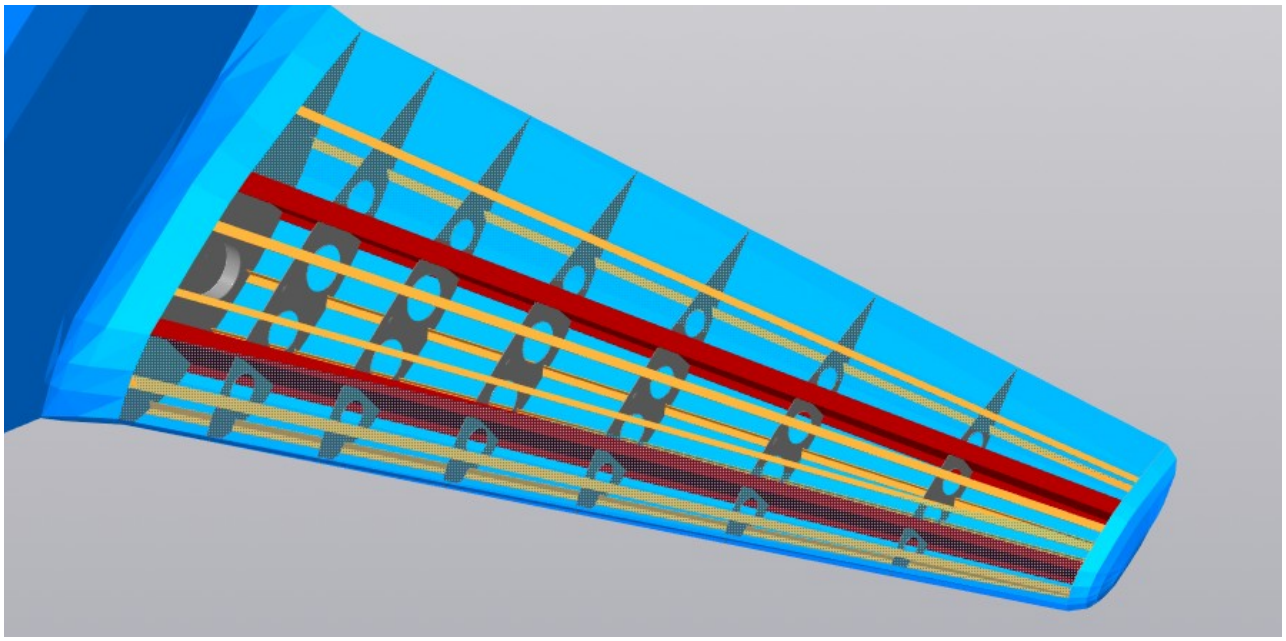

Fig. 11. Construction of the power set of the LA wing

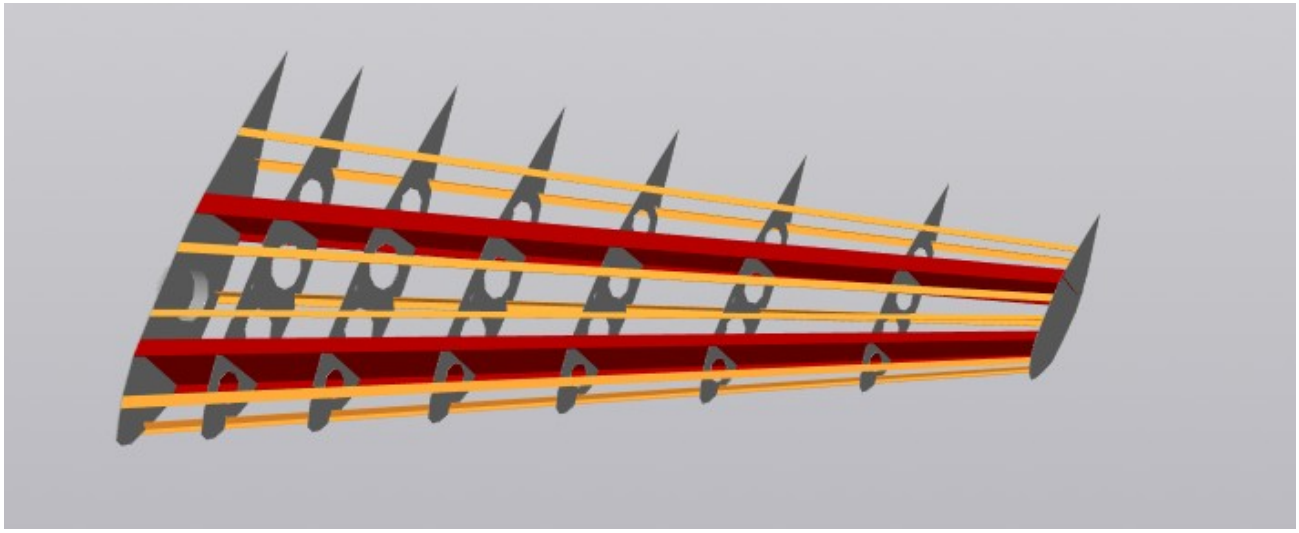

Fig. 12. Power set of LA wing (stringers, ribs, spars)

Fig. 13. General view of the glider with feathers and power elements

					АЛ9412.06.00.00.00EN	Sheet
Ch.	Sheet	N document	Sign.	Date		

Fig. 14. Construction of the front rack of the chassis

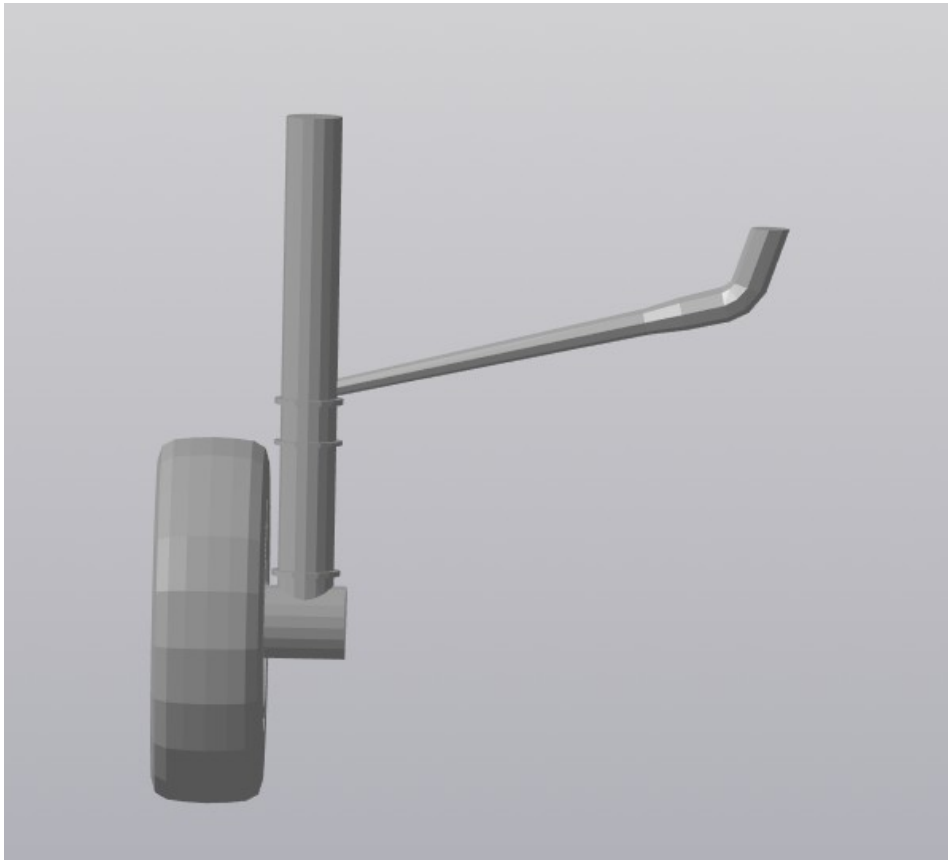

Fig. 15. Construction of the main rack of the chassis with a brace

					АЛ9412.06.00.00.00EN	Sheet
Ch.	Sheet	N document	Sign.	Date		

Conclusion on the chapter

Structural modeling was performed in Creo Parametric. All the main elements of the design were developed separately, after which they were included in the general assembly. To create a spatial model, it is first necessary to create a theoretical surface, then, depending on the type of part, using tools such as drawing, bending, etc. we perform the necessary operations to obtain the part.

3. Research of loads structures

During the flight of an unmanned aircraft, it is under the influence of certain vacuum and pressure forces, which are evenly distributed over the wing skin. The wing is also affected by mass forces of the wing structure itself, distributed evenly over its span, as well as certain concentrated forces in the form of aggregates or loads.

According to airworthiness standards, we accept the operational overload $n^э = 3$ and the safety factor $f = 1.5$.

The wing of an unmanned aircraft is straight and has a trapezoidal shape. The length of the cantilever together with the part of the center plane that creates the lifting force is 5.2 m. For calculations, this part of the wing was divided into 12 parts, the length of each of which is $\Delta z = 0.433$.

For further calculations of the torque of the wing, we need to know such a parameter of the wing as the center of its stiffness $X_{Ц.Ж.}$, while assuming in advance the shading of the centers of distribution of mass forces X_M (0.42 chord length) and the centers of distributed aerodynamic forces $X_Д$ (0.2 chord length).

$$X_M = 0,42 \cdot b$$

$$X_Д = 0,2 \cdot b$$

$$X_{Ц.Ж.} = \frac{H_1^2 * x_1 + H_2^2 * x_2}{H_1^2 + H_2^2} = \frac{(0,08b)^2 * 0,15b + (0,04b)^2 * 0,75b}{(0,08b)^2 + (0,04b)^2} = 0,27b$$

where where b is the chord length of the wing section , H_1 - height the front spar (we accept for 0.08 b) , H_2 - height _ rear spar (we accept for 0.04 b) , x_1 - placement the front spar relatively front edges wings (we accept for 0.15b) , x_2 - accommodation rear spar (we accept for 0.75b) .

We define the distributed load on the wing as follows:

$$q_{пов} = \frac{m_0 \cdot n^e \cdot f}{S} \cdot b$$

where S is the area wings _

Distributed mass load let's define as follows :

$$q_{мас} = \frac{m_{кр} \cdot n^e \cdot f}{S} \cdot b$$

Mass and aerodynamic load replace with one equivalent load :

$$q = q_{пов} - q_{мас}$$

For further buildings we need epur find transverse force, bending and twisting moments in each section wings _

The value of transverse strength in the selected section of the wing will be determined as follows :

$$Q_i = \sum_{i=1}^{n} (\Delta Q_i - m_{ван\,i}) = \sum_{i=1}^{n} ((q^p_{ср\,i} \cdot \Delta z) - m_{ван\,i}) =$$

$$= \sum_{i=1}^{n} (((\frac{q_i + q_{(i+1)}}{2}) \cdot \Delta z) - m_{ван\,i})$$

where n is the number plots , on which broken half-span , $q^p_{ср\_i}$ - average value running load on to each area in length Δz , ΔQ_i - increase transverse strength on any area wings (for an exception final areas where _ $\Delta Q_{кінц} = \frac{2}{3} \cdot q_1 \cdot \Delta z$, where q_1 - running load in the first sections wings from the end

The magnitude of the bending moment is determined as follows:

$$M_{згин\,i} = \sum_{i=1}^{n} \Delta M_{згин\,i} = \sum_{i=1}^{n} Q_{ср\,i} \cdot \Delta z = \sum_{i=1}^{n} \frac{Q_i + Q_{(i+1)}}{2} \cdot \Delta z$$

where $\Delta M_{згин\,i}$ is the increase bending moment.

The value of the torque is determined as follows:

$$M_{кр\,i} = \sum_{i=1}^{n} (\Delta M_{кр\,i} - M_{кр\,вани}) = \sum_{i=1}^{n} ((m_{ср\,i}^{p} \cdot \Delta z) - M_{кр\,вани}) = \sum_{i=1}^{n} (((\frac{m_i + m_{i+1}}{2}) \cdot \Delta z) - M_{кр\,вани}),$$

where $\Delta M_{кр\,i}$ is the increase of torque in any sections , $m_{ср\,i}^{p}$ - the average the value of the running torque on each area , $m_i = q_{пов} \cdot (X_{Ц.Ж.} - X_{Д}) + q_{мас} \cdot (X_M - X_{Ц.Ж.})$ - uniform torque , where $X_{Ц.Ж.} - X_{Д}$ is the distance from the center of pressure to the line centers bend , $X_M - X_{Ц.Ж.}$ - distance from center of mass line wings to the line centers of bending , and $M_{кр\,вани} = p \cdot h_{дв} - m_{дв} \cdot a_2$ (h $_{dv}$ – distance from the center of mass of the engine to the vertical center of rigidity , a $_2$ is the distance from the center of mass of the engine to the center of rigidity horizontally).

On the basis of the above calculations, we summarize the results in a table and based on them, we build charts of force factors acting on the wing.

Table 1.

Distributed aerodynamic load

Table 2

section no	bi, m	q pov ., kgf /m	q mass , kgf /m	q, kgf / m
1	0.78	1070	182	888
2	0.8694	1193	203	990
3	0.9588	1315	224	1092
4	1.0482	1438	244	1194
5	1.1376	1561	265	1295
6	1,227	1683	286	1397
7	1.3164	1806	307	1499
8	1.4058	1929	328	1601
9	1.4952	2051	349	1703
10	1.5846	2174	370	1804
11	1,674	2297	390	1906
12	1.7634	2419	411	2008
13	1.8528	2542	432	2110

Transverse force

section no	bi, m	ΔZ, m	qi, kgf / m	qi+1, kgf / m	ΔQi, kgf	Qi, kgf
1	0.78	0.43	888	990	257	257
2	0.87	0.43	990	1092	407	663
3	0.96	0.43	1092	1194	451	1115

4	1.05	0.43	1194	1295	495	1610
5	1.14	0.43	1295	1397	539	2149
6	1.23	0.43	1397	1499	583	2732
7	1.32	0.43	1499	1601	627	3360
8	1.41	0.43	1601	1703	672	4031
9	1.50	0.43	1703	1804	716	4747
10	1.58	0.43	1804	1906	760	5507
11	1.67	0.43	1906	2008	804	6311
12	1.76	0.43	2008	2110	848	7159
13	1.85	0.43	2110	-	892	8051

Table 3

Bending moment

section no	**bi, m**	**ΔZ, m**	**Qi, kgf**	**Qi+1, kgf**	**ΔMi, kgf *m**	**Mi, kgf *m**
1	0.78	0.43	257	663	0	0
2	0.87	0.43	663	1115	199	199
3	0.96	0.43	1115	1610	385	585
4	1.05	0.43	1610	2149	590	1175
5	1.14	0.43	2149	2732	814	1989
6	1.23	0.43	2732	3360	1057	3047

7	1.32	0.43	3360	4031	1320	4366
8	1.41	0.43	4031	4747	1601	5968
9	1.50	0.43	4747	5507	1902	7869
10	1.58	0.43	5507	6311	2221	10091
11	1.67	0.43	6311	7159	2560	12651
12	1.76	0.43	7159	8051	2918	15569
13	1.85	0.43	8051	-	3295	18864

Table 4.

A turning point

section no	**bi, m**	**ΔZ, m**	**mkri , kgf *m**	**mcri+1, kgf *m**	**Δ Mcri , kgf *m**	**Mcri , kgf *m**
1	0.78	0.43	80	99	0	0
2	0.87	0.43	99	120	39	39
3	0.96	0.43	120	144	48	86
4	1.05	0.43	144	170	57	144
5	1.14	0.43	170	197	68	211

6	1.23	0.43	197	227	79	291
7	1.32	0.43	227	259	92	383
8	1.41	0.43	259	293	105	488
9	1.50	0.43	293	329	120	608
10	1.58	0.43	329	367	135	742
11	1.67	0.43	367	407	151	893
12	1.76	0.43	407	450	168	1061
13	1.85	0.43	450	-	186	1247

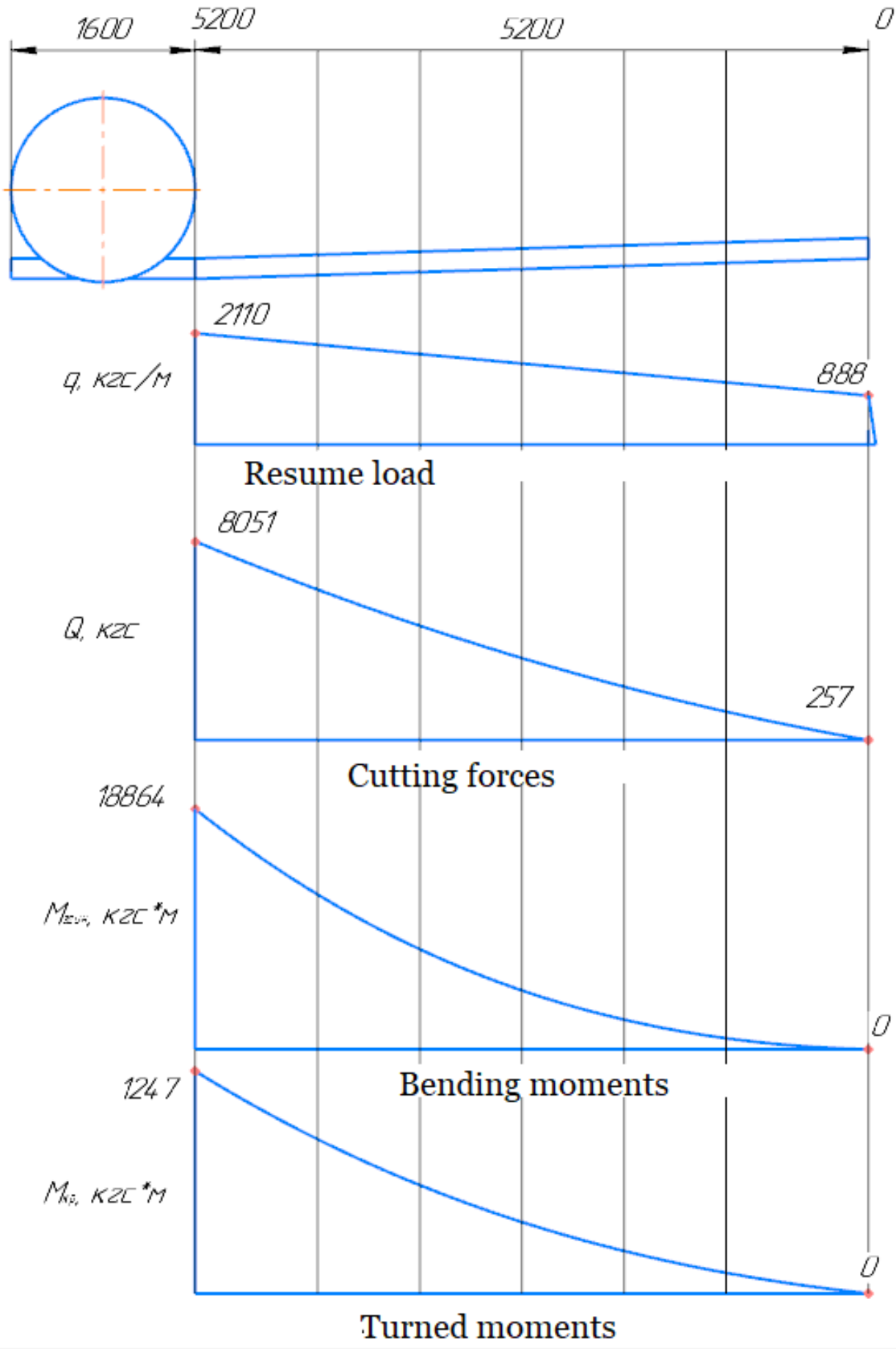

Fig. 16. Plots of force factors acting on the wing

					АЛ9412.06.00.00.00EN	Sheet
Ch.	Sheet	N document	Sign.	Date		

Conclusion on the section

In this section, calculations were carried out distributed in the wing skin of the developed glider, in particular, the distributed aerodynamic load, transverse forces, bending moment and torque were calculated. Based on the obtained results, diagrams of force factors acting on the wing were constructed.

4. Aerodynamic calculation of an unmanned aircraft

Aerodynamic analysis of the powerful thrust method is convenient to do for higher performance aircraft, since the main characteristic of their plant is thrust. A simplified analysis by the thrust method , found on the graphs, the required P and the available Pp of the horizontal power in the course of the speed from the speed at different heights. In fig. as soon as possible, the graphic plot looks at full height on the level. This graph shows how fast they are V $_{min}$, V $_{ec}$, V $_{max}$. With the help of this graph, it is possible to quickly establish the range of speed and maximum excess momentum ΔP_{max}, which, as noted, is located between the speeds Vnv . and Old .

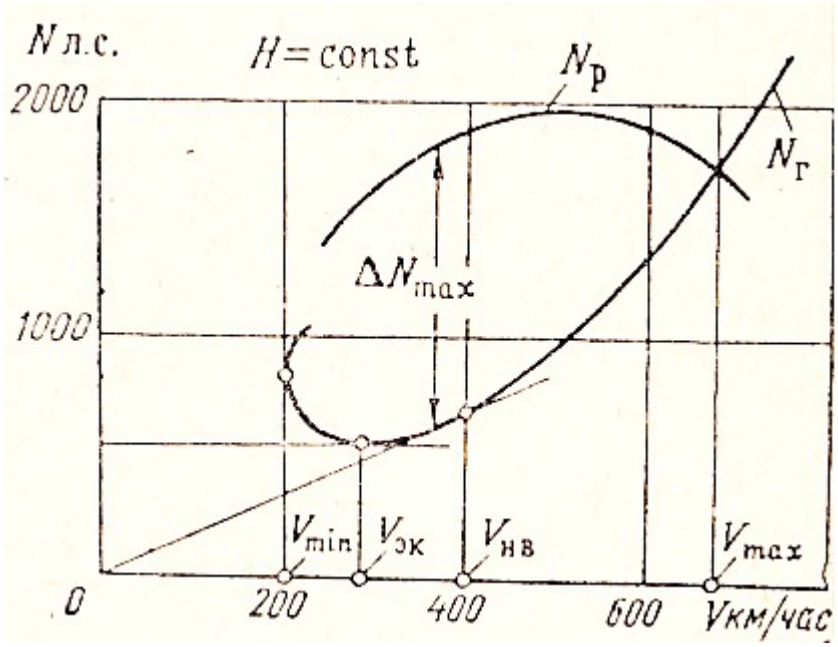

Fig. 17. Curves F g and Np LA.

Excess power, like excess thrust, is used to gain altitude and increase airspeed. In constant horizontal flight, excess power is not used, for this the engine is suppressed.

To determine the flight characteristics of the aircraft at different altitudes, a combined graph of the required and available thrust at altitudes is constructed.

In this case, in high-altitude injection engines up to the calculated altitude Hp , it increases and falls above this altitude.

It can be seen, for aircraft with high-altitude engines equipped with a supercharger, these characteristics of the design height Hp of the engine increase, and above this altitude -decreases .

The following graph is shown for aircraft with low-level and high-level engines. From this graph, it can be seen that the vertical speed of an unmanned aircraft with a low-mobility engine decreases all the time as the altitude increases, while an aircraft with a high-altitude engine increases to the design altitude and falls above the design altitude. Therefore, at the same vertical speed in the ground, the ceiling of a drone with a high-altitude engine is much higher than that of a drone with an engine at low altitude. To construct the ascent barogram, the graph of the dependence $V_{ymax}=\varphi(H)$is rearranged into the graph of the dependence $1 / V_{ymax}=\varphi(H)$, after which the time of acquisition of each section of height is found by the method of graphic integration.

Calculations are carried out according to the same table as in the rod method. According to the data in the table, barograms of ascent are built.

For the developed unmanned aircraft, the flight height is 11 km. The required power Vek = 600 hp , the available power of two engines is 1400 kN , which is enough for a reconnaissance drone.

The flight range is the distance along 1 horizontal plane flying on the plane, moving it in one vertical plane after consuming a certain amount of fuel. This distance includes the following areas typical of flight range calculations:

- the area traveled by the aircraft at a given altitude;
- the main section corresponding to a horizontal flight at a given height;
- the area traveled by the plane when it descends to land at the destination.

To simplify the calculations, we will not take into account the Ch. in flight weight due to fuel burnout, and we will assume that in the second, main section, the aircraft has a constant flight weight and a constant speed. The distance

traveled by the aircraft on the main section is usually up to 95% of the full range. This distance, determined in the absence of wind, is called the technical range.

In the future, we will limit ourselves to the presentation of the method of calculating the range and duration of the flight for the main section. The supply of fuel to the aircraft corresponding to the technical range of its flight is called the available fuel supply.

Available fuel is equal to the full fuel reserve minus the portion required to start and test the engines before flight, circle after takeoff and above the destination aerodrome, establish a target altitude, and lower the aircraft for landing.

In addition to the technical range, a distinction is made between the practical range of the flight, meaning by this term the distance along the horizon traveled by the aircraft after consuming the available fuel supply, minus the so-called aeronautical fuel supply.

Aeronautical fuel supply is determined by the conditions when boldly reducing the range of wind gusts and when bypassing mountains, thunderstorms, clouds, etc. Obstacles. Usually it is 5 ÷ 10% of the total amount of fuel. Sometimes the concept of the range of an aircraft is used, that is, the maximum distance an aircraft can travel from its airfield, provided it returns to it without intermediate landings and refueling.

The flight range depends on the following main factors: fuel supply, number of kilometers of fuel consumption, tortuosity and pitch in the flight mode (speed and altitude), direction and strength of the wind on the flight route. The time that an aircraft can stay in the air before the available fuel is completely exhausted is called the duration of the flight.

Technical flight range is determined by the formula

$$L = \frac{G_{m.p}}{q_к}$$

where L is the flight range in km;

$q_к$— fuel consumption per kilometer in kg/km;

$G_{m.p}$— available fuel stock in kg.

The duration of the flight depends on the supply of fuel to the aircraft and its hourly consumption is determined by the ratio

$$T = \frac{G_{m.p}}{q_ч}$$

where T is the flight duration in hours;

$q_ч$- hourly fuel consumption in kg/h.

Range and flight duration formulas for aircraft with jet engines

The expanded formula that determines the flight range is obtained from the formula as follows.

It is known that fuel consumption per kilometer

$$q_k = \frac{q_ч}{3.6 V_H} [kg/km]$$

where V is the flight speed at a given height in m/ sec , and is the hourly consumption

fuel

$$q_ч = c_e P_e [kg/km]$$

where Ce is the specific fuel consumption in kg/l. with. h., i.e. fuel consumption by the engine (or engines, if there are several on the plane) per unit of power in one hour.

For modern jet engines

$$c_e \approx 1{,}00 \div 1{,}2 \frac{kg}{kgs\,hour}.$$

Pe — effective thrust of the engine (or engines) in l. with.
Since the technical range is determined under conditions of horizontal flight, the thrust required for flight should be equal to the known one.

$$P_e = \frac{G_{cp}}{K}$$

.
where Pe is the thrust of the engine, K is the quality of the unmanned aircraft
Gcp - average flight weight in kg.
This weight is determined as the difference between the initial flight weight of the unmanned aircraft at takeoff Go and the arithmetic mean of the sum of the weights of the available fuel Gt.p (burned in flight) reset in
cargo flight G_{cp}.

$$G_{cp} = G_0 - \frac{G_{m.p} + G_{сб}}{2}$$

By substituting the found expressions for $q_k$and Pe, we obtain from the formula

$$L = \frac{G_{m.p}}{q_k} = \frac{G_{m.p} 3{,}6 V_H}{q_ч} = \frac{G_{m.p} 3{,}6 V_H}{c_e P_e} = \frac{G_{m.p} 3{,}6 V_H}{c_e Gcp / K}$$

or

$$L = 3{,}6 \frac{G_{m.p} K V_H}{G_{cp} c_e}$$

It can be seen from the formula that the flight range depends on wear $\frac{G_{m.p}}{G_{cp}}$,

which is a constant value independent of the flight mode and the value of the

variable K, $K \frac{V_H}{c_e}$ dependent on the flight mode.

The maximum flight range is obviously achieved at the maximum value of $K \frac{V_H}{c_e}$

.

The speed at which the maximum range is reached is called the cruising speed. For aircraft at cruising speed

$$V_{cruis} \approx (0{,}85 \div 0{,}9) V_{max}$$

The flight range at the maximum value of the speed is approximately 50% of the cruising speed.

The formula for flight duration can be expressed, more fully, as follows.

Similarly with the flight range, recording the duration of the flight

$$T = \frac{G_{m.p}}{G_{cp}} \frac{K}{c_e} \text{ [hours]}$$

Under conditions of constant relative flight duration, which would be achieved at the most economical speed .

Thus, reducing the aircraft will significantly increase its flight range and reduce the requirements for production facilities

The take-off weight of the aircraft in the first approximation:

¿

where

$m_{ц.н.}$ = 1000 kg – the mass of the target (payload) load;

$\overline{m}_{кон}$ = 0.25 – the relative mass of the structure (the mass of the structure is related to the take-off mass mkon/m0);

$\overline{m}_{с.у.}$ = 0.08 – relative mass of the power plant;

$\overline{m}_{сист.}$ = 0.08 – relative mass of aircraft systems;

$\overline{m}_{пал}$ = 0.3 – relative mass of fuel.

$\overline{m}_{кон}$, $\overline{m}_{с.у.}$, $\overline{m}_{сист.}$, $\overline{m}_{пал}$ - values are determined according to table 2.1.

$m_{сл}$ - weight of service load, equipment and supplies;

Weight of aircraft equipment:

$m_{об} = (0,03..0,05) \cdot m_0^{cm}$ =240 kg - for aircraft from $m_0^{cm} < 6$ т;

$m_0^{cm} = (m_0^1 + m_0^2 + m_0^3 + m_0^4)/4 = 6000$ kg

m_0^1, m_0^2, m_0^3, m_0^4 – take-off masses of selected analogues.

The mass of special equipment:

$m_{\text{special equipment}} = (0,03..0,05) \cdot m_{0\,ст}$=240 kg

Aircraft equipment includes:

- aeronautical (instruments, remote controls, autopilot);
- electrical equipment (generators, batteries, energy converters, wiring, fittings);
- radio equipment (radio communication equipment, radio navigation, radar equipment, automatic take-off-landing systems);
- hydropneumatic (energy sources, working fluid and compressed air, tanks, cylinders, communications fittings);
- fire protection and ice formation prevention system;

Special equipment includes:

- devices for dropping cargo in flight;
- sights, guidance systems, weapons, photographic equipment

Table 5.

Relative masses of aircraft components

Destination of the aircraft		$\overline{m}_{кон}$	$\overline{m}_{с.у.}$	$\overline{m}_{сист.}$	$\overline{m}_{пал}$
Military transport and cargo	light	0,25 .. 0,27	0,08 .. 0,09	0,07 .. 0,08	0,20 .. 0,25
	medium	0,21 .. 0,23	0,07 .. 0,08	0,06 .. 0,07	0,25 .. 0,30
	heavy	0,23 .. 0,27	0,05 .. 0,06	0,04 .. 0,05	0,30 .. 0,35

Table values $\overline{m}_{пал}$ 2.1 are indicative, since the relative mass of fuel depends on the calculated values of the range Lp or the flight time tp. Therefore, the data in the table. 2.1 for $\overline{m}_{пал}$ is recommended to be adjusted by the formula::

$\overline{m}_{пал} \approx a + b \cdot t_p = a + b \cdot L_p / V_{крейс} = 0,3$

a = 0,03 ... 0,04 for light maneuverable aircraft (m_0<5700 kg);

a = 0,05 ... 0,06 for all other aircraft;

b = 0,04 ... 0,05 for subsonic aircraft;

Smaller values of the coefficient b correspond to larger tonnage aircraft.

The supercritical airfoil (Fig. 2.2) is a subsonic wing airfoil, which allows for a fixed value of the lift force coefficients and profile thickness to significantly increase the critical Mach number. These profiles are intended primarily for wave drag delay in the transonic speed range. For a flight speed of Mach 0.8-0.9 (depending on the flight height), a supercritical airfoil - SC(2)-0714 with a relative thickness of 13.9% will be used.

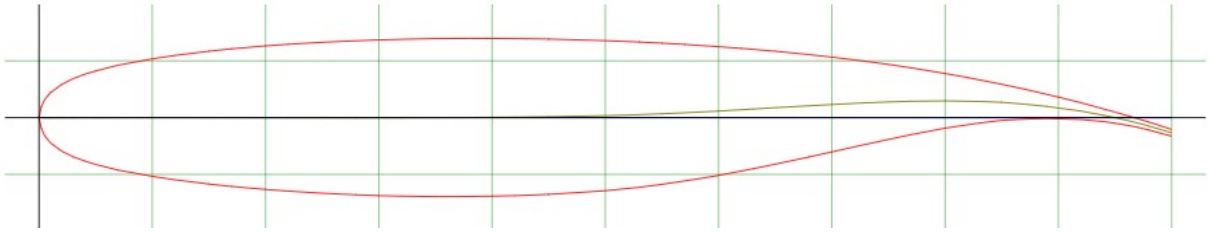

Fig.18. Supercritical airfoil SC(2)-0714

Definition of general geometric parameters of the wing

1. The wing area is determined by the formula:

$$S_{кр} = \frac{m_0}{p_{num}} = \frac{5103}{430} = 11,86\ м^2$$

where:

m_0 – take-off mass of the aircraft in the first approach, kg

p_{num} – the average specific load on the wing, kg/m2, is determined by the statistics of the prototypes:

$p_{num} = 430\ кг/м^2$

Based on the statistical data of analogues and in accordance with the selected aerodynamic scheme, we set in the first approximation the value:

$\lambda_{кр}$= 5,4 wing extension

$\eta_{кр}$= 3,5 wing narrowing

χ=30° wing arrow-likeness

1. Wing span

$l_{кр} = \sqrt{\lambda_{кр} \times S_{кр}} = 8\,м$

2. End chord of the wing

$b_{кц} = \frac{2 \times S_{кр}}{l_{кр} \times (1 + \eta¿¿кр)} = 0{,}65\,м¿$

2. Root chord of the wing

$b_0 = \eta_{кр} \times b_{кц} = 3{,}5 \times 0{,}65 = 2{,}275\,м$

2. Determination of the middle aerodynamic chord by a graphical method

САХ = 1,36 м

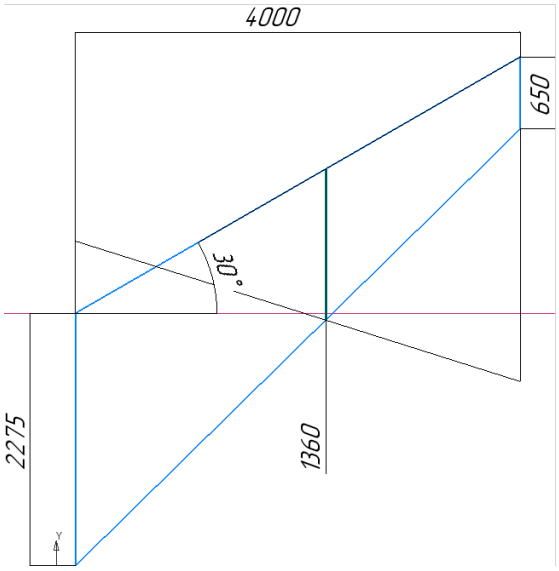

Fig.19. Middle aerodynamic chord determination

The relative elongation of the horizontal tail (GO) at this stage is chosen based on the analysis of statistical data $\lambda_{GO} = 3$.

We accept the narrowing of the GO as equal $\eta_{GO} = 3$

Square of GO: $S_{ГО} = \frac{A_{ГО} \cdot S_{кр}}{\bar{L}_{ГО}} = \frac{0{,}75 \cdot 11{,}86}{3} = 2{,}965\,м^2$

Span of GO: $l_{ГО} = \sqrt{\lambda_{ГО} \cdot S_{ГО}} = \sqrt{3 \cdot 2{,}965} = 2{,}98\,м$

$b_{кц} = \frac{2 \times S_{ГО}}{l_{кр} \times (1 + \eta_{ГО})} = \frac{2 \times 2{,}965}{2{,}98 \times (1+3)} = 0{,}5\,м$

$b_0 = \eta_{ГО} \times b_{кц} = 3 \times 0{,}5 = 1{,}5\,м$

Square of vertical tail BO: $S_{BO} = \frac{A_{BO} \cdot S_{кр}}{\bar{L}_{BO}} = \frac{0{,}07 \times 11{,}86}{(3 \times 1{,}36/8)} = 1{,}627\,м^2$

The relative elongation of the vertical tail (VO) at this stage is chosen based on the analysis of statistical data $\lambda_{BO} = 3$.

The narrowing of the VO is taken as equal $\eta_{BO} = 3$

We accept the angle of wing arrow-likeness of BO by ¼ chords BO $\chi_{0,25} = 40°$.

The height of the double BO: $h_{BO} = \sqrt{\lambda_{BO} \times \frac{1}{2} \times S_{BO}} = \sqrt{3 \times \frac{1}{2} \times 1{,}627} = 1{,}56\ м$

$$b_{кц} = \frac{S_{BO}}{h_{BO} \times (1+\eta_{BO})} = \frac{1{,}627}{1{,}56 \times (1+3)} = 0{,}26\ м$$

$$b_0 = \eta_{BO} \times b_{кц} = 3 \times 0{,}26 = 0{,}78\ м$$

Based on the calculations made above, a preliminary model of the UAV was created

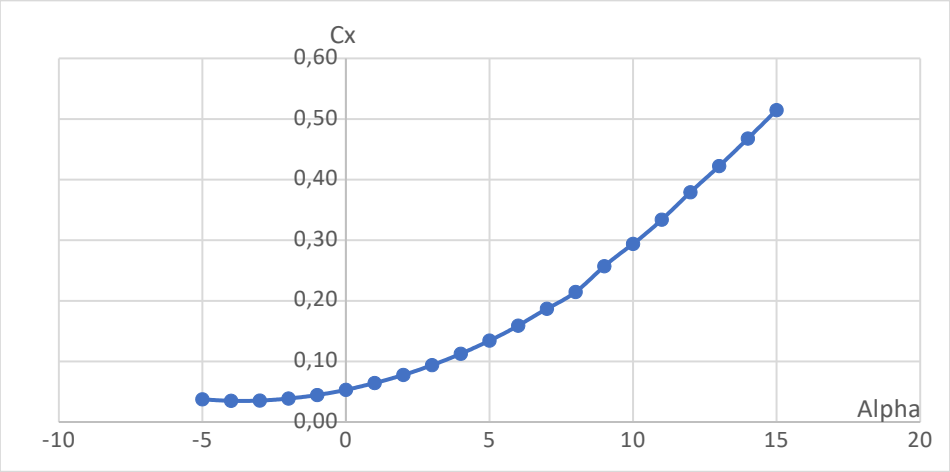

Fig. 20. Graph of the dependence of the coefficient of resistance on the angle of attack

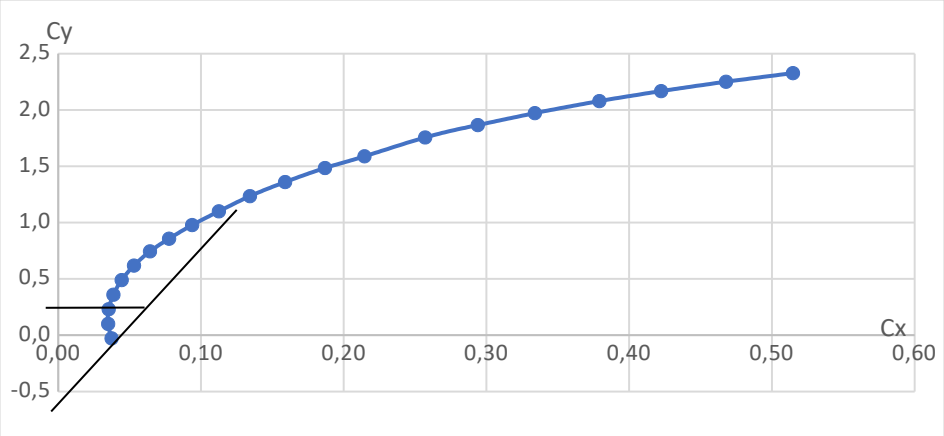

Fig. 21. The graph of the dependence of the lift force coefficient on the drag force coefficient

					АЛ9412.06.00.00.00EN	Sheet
Ch.	Sheet	N document	Sign.	Date		

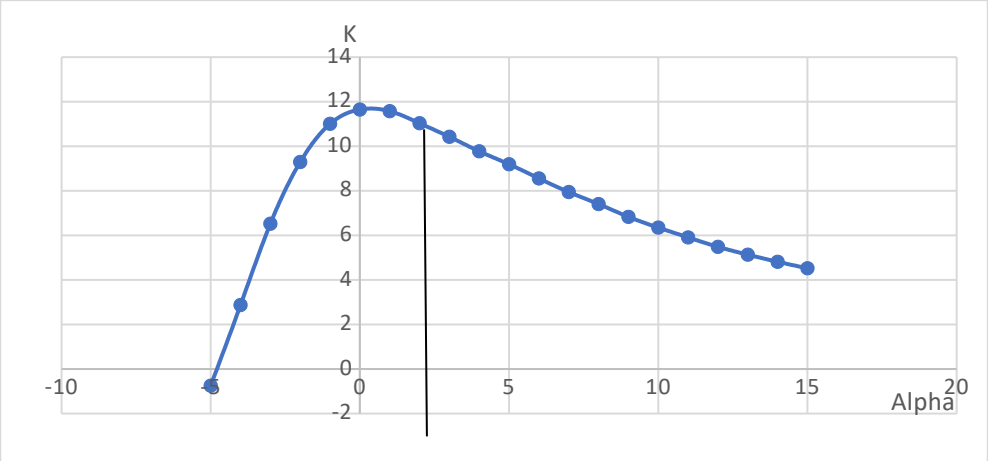

Fig. 22. Graph of the dependence of aerodynamic perfection on the angle of attack

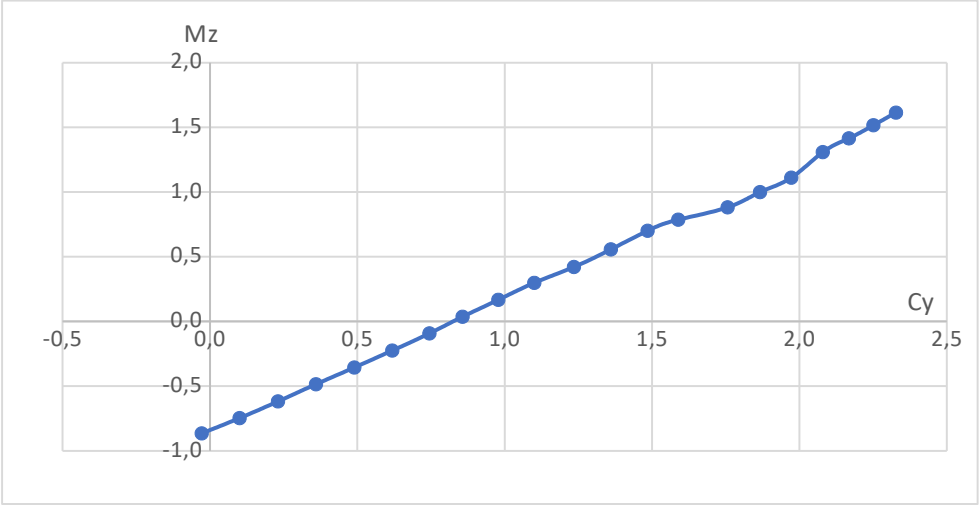

Fig. 23. The graph of the dependence of the longitudinal moment on the lift coefficient

Intersection of the moment graph with zero (Fig. 29) at Cy = 0.8, which corresponds to an angle of attack of approximately 2 degrees (Fig. 25). this value of the angle of attack is close to the angle of the highest aerodynamic quality (Fig. 28) for this form of aircraft. With further optimization of the aerodynamic shape of the aircraft, it is possible to achieve the coincidence of the quality point and the balancing point.

The design flight range of the UAV is about 2,000 km, the useful load is up to 1 ton, the cruising speed is 1,000 km/h.

With an aircraft weight of 3,400 kg, the fuel weight is 1,020 kg

Fuel consumption in cruising flight mode: 220 kg/h

1020/220=4.6 hours of flight at 1000 km/h

That is, it turns out 4.6*1000=4600 km

A cruise flight speed of 1000 km/h was selected according to the Zhukovsky curve (Fig. 24) for a thrust of 400 kgf in cruise mode of the AI-25 engine at an altitude of 10 km. At the same time, the minimum speed required for landing remains 200 km/h.

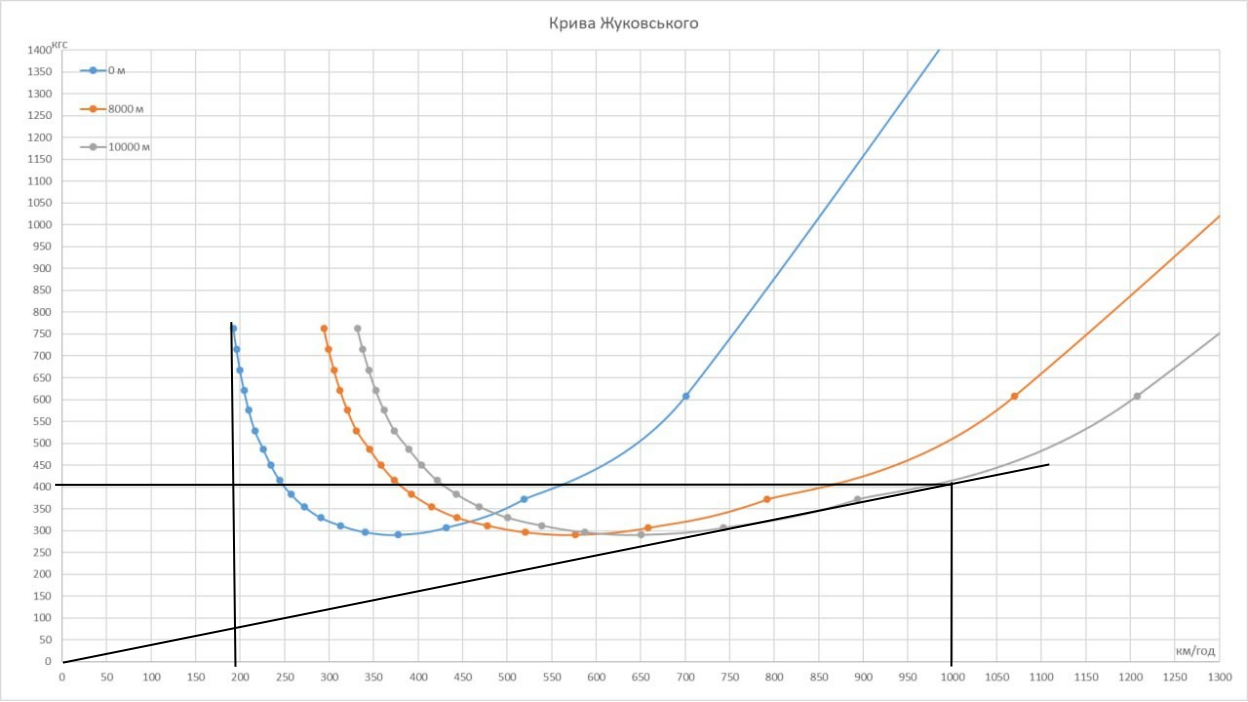

Fig. 24. The graph of the dependence of the required power on the flight speed

Conclusion on the section

Calculation using the grapho-analytical method allowed to obtain the optimal parameters of a reactive UAV, the main ones of whichIn total, it will be approximately 4000 km, taking into account that more fuel will be spent on take-off and landing. payload mass 600 kg.

5. Calculation of wing resource

During the Nastran 2018 system was used for calculations .

Let 's build a load model . Cyclic in flight from flow disruption the load will be damping . Observations were made and it was determined that during the flight there is an observation noticeable _ fluctuation periodically , once every 1 minute for ten cycles with the frequency of oscillations from 0.5 Hz to 2 Hz. Amplitude fluctuations noticeable , so it is approximately 0.25... 0.5 m. Wing span - 1 2 meters _ Duration flight to the landing point - 4 hours . Takeoff weight of the drone of the plane - 3300 kg .

Knowing how to walk critical _ point and actions load _ In particular , apply to the wing end caisson load of 100 kgf (Fig. 19).

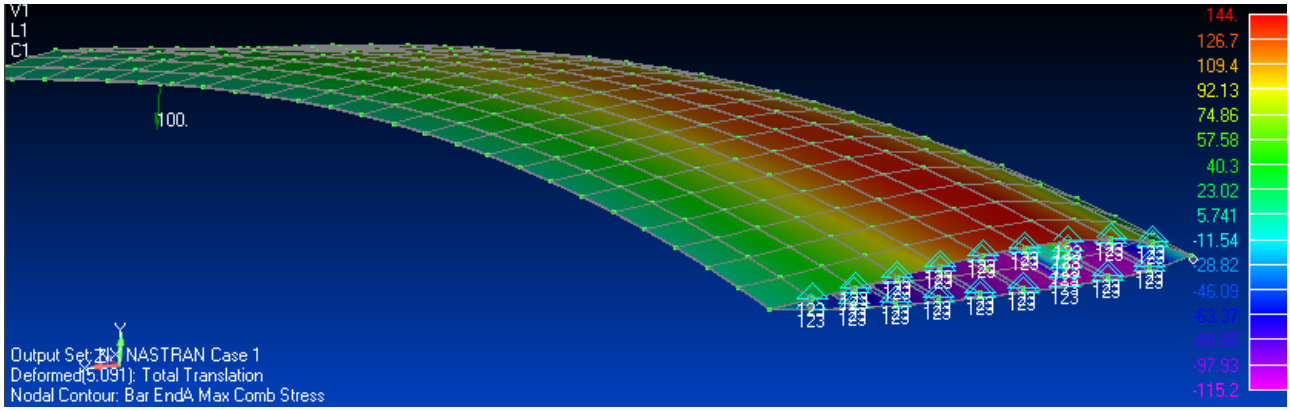

Fig. 25. Mechanical stresses in rod elements

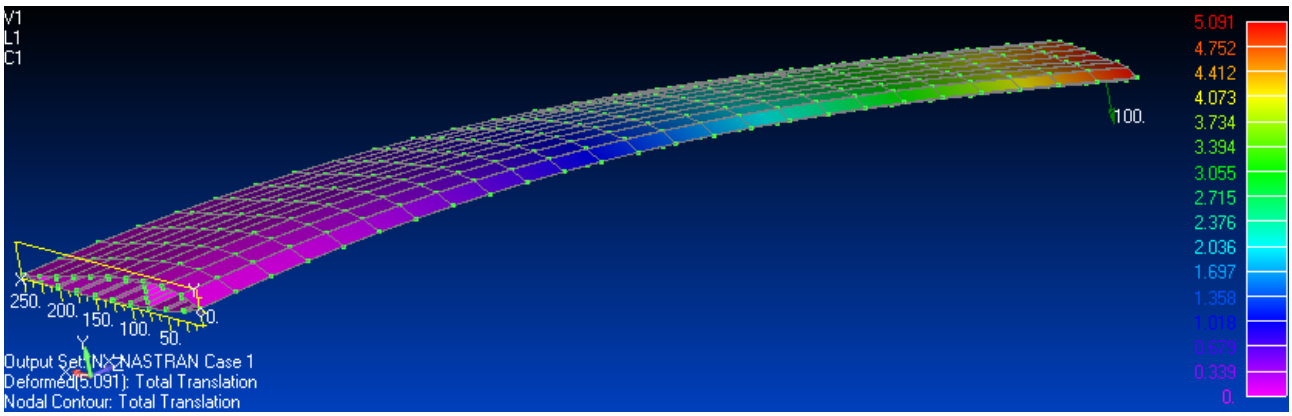

Fig . 26 . Relocation wings

Moving is equal to δ=5 cm , mechanical stress σ_{eqv} , therefore for the fourth theory strength (Huber-Mises-Genka)

$$\sigma_{eqv} = 0.7 ((\sigma_1 - \sigma_2) + (\sigma - \sigma) + (\sigma - \sigma))^{0.5} = 150 \text{ kgf/cm}^2,$$

where σ 1, σ 2, σ 3 - the main ones voltage _ along mutually perpendicular axles _

The same voltage module also occurs in two-node elements (Fig. 25. Bar End A Max Comb Stress) . In case of 10 times displacement more greater than δ' = 50 cm, the mechanical stresses will be σ' = 1500 kgf /cm ^{2} . The biggest voltage belong to the elements near root and ribs , corresponding here expedient to choose critical point (in the spar belt).

According to the formula Serensena-Kinasoshvili , equivalent High-voltage symmetrical cycle

$$\sigma_{a\,eqv} = \sigma_a + \psi_\sigma \sigma_m \qquad (3)$$

where σ_a , σ_m – amplitude and average tension specified asymmetric load cycle , ψ_σ is the coefficient asymmetry of the load cycle , which is determined by the formula

$$\psi_\sigma = (2 \sigma_{-1} - \sigma_0) / \sigma_0 \qquad (4)$$

Here σ_{-1} is the limit endurance for a symmetrical load cycle _ ($\sigma_m = 0$), σ 0 is the limit endurance by pulsating th cycle in load ($\sigma_a = \sigma_m$).

Load under selected conditions symmetrical relative to the zero position in time , respectively

$$\sigma_m = 0, \text{ and } \sigma_{a\,eqv} = \sigma_a = \sigma_{eqv} .$$

The border endurance σ_D element developed design

$$\sigma_D = K_D \sigma_{-1} \qquad (5)$$

where K_D is the coefficient impact structural element , which determined by the formula:

$$K_Д = \frac{1}{(K_\sigma / K_d + 1/K_F - 1)/K_v}, \qquad (6)$$

where K_σ - effective coefficients concentration stress (reduction of endurance limits of the main sample to the limit endurance of a sample with a voltage concentrator), is calculated according to the formula

$$K_\sigma = 1 + (\alpha_\sigma - 1)\, q\,. \qquad (7)$$

α_σ – the theoretical coefficient of stress concentration, achieved by nomograms, q is the coefficient of sensitivity of the material to the concentration of stress, we choose the value q = 0.4 required for aluminum ;

Kd - the coefficient contained in the free size, section or scale factor (reduction of the endurance limit of the diagram sample to the endurance limit of the sample with a standard diameter), which exists on the nomogram; KF is a coefficient used only in age (reduction of endurance limits with a break with the determination of who trusts the endurance limit with a break, at the moment when the Weller curve is obtained), used in the nomogram, Kv is a coefficient that limits the vitrification of the sample to only the necessary . to the limit of endurance does not Ch. the cut), which is calculated using nomograms .

When performing calculations are valid options in the formula Ch.s replacement voltage amplitudes σ_{a}_ need Fr make a substitution

$$\sigma_{aD} = \sigma_{a} / K_{D}$$

For example , formula (3) will yield view :

$$\sigma_{a\,eqv} = \sigma_{a} / K_{D} + \psi_{\sigma} \sigma_{m} \qquad (8)$$

Damage , storage in a safe points researched structures in the tasks conditions be considered according to the formula

$$\psi = \sum_{i=1}^{N_b} \psi_i = \sum_{i=1}^{N_b} \frac{k_i}{N_i}, \qquad \psi_i = \frac{k_i}{N_i}. \qquad (9)$$

k_i - quantity cycles given amplitudes , Ni is the maximum number of such cycles .

In case description process accumulation damage equation (9) condition destruction registered as:

$$\psi \geq and_{R.} \_ \qquad (10)$$

where and_{P} *is* a number close to "1".

Calculation of the theoretical coefficient concentration tension in CAD systems and Nastran .

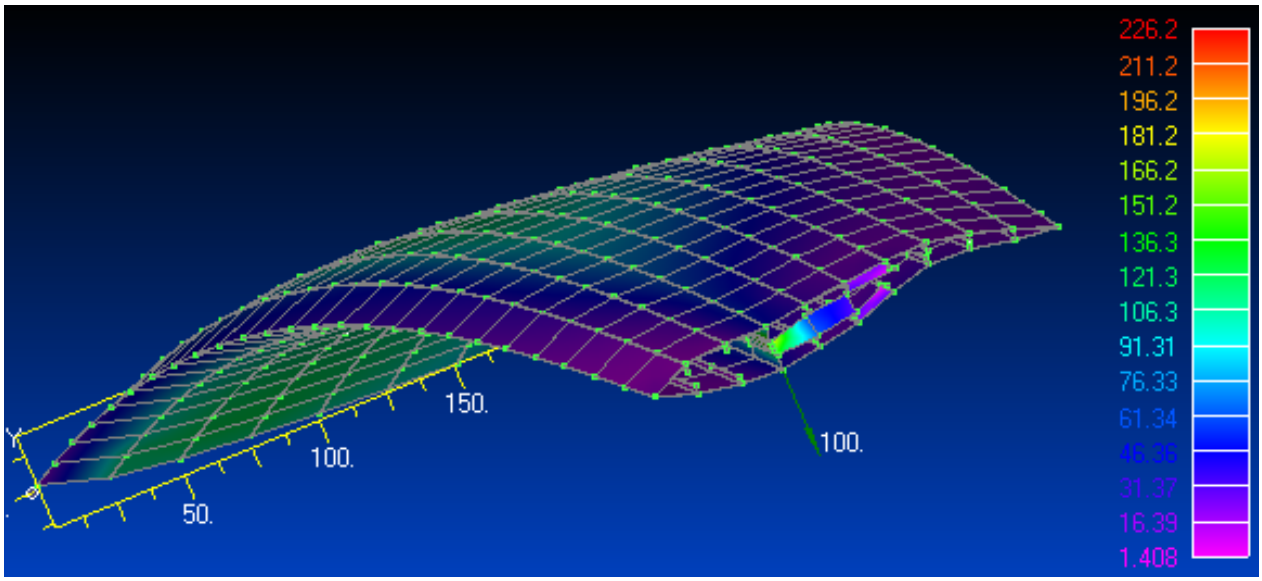

Fig. 27 . Distribution stresses on the profile , with by involving indicators of its concentration in the elements

Definition the coefficient of concentration stresses :

$$\alpha_\sigma = \sigma_{nom} / \sigma_{max} = 1500 / 2260 = 0.67. \quad (11)$$

Coefficient impact quality processing surface at the limit stability for the belt of the spar $\sigma_T = 350$ MPa (aluminum from a rolled profile) , corresponds to the value F = 0.8.

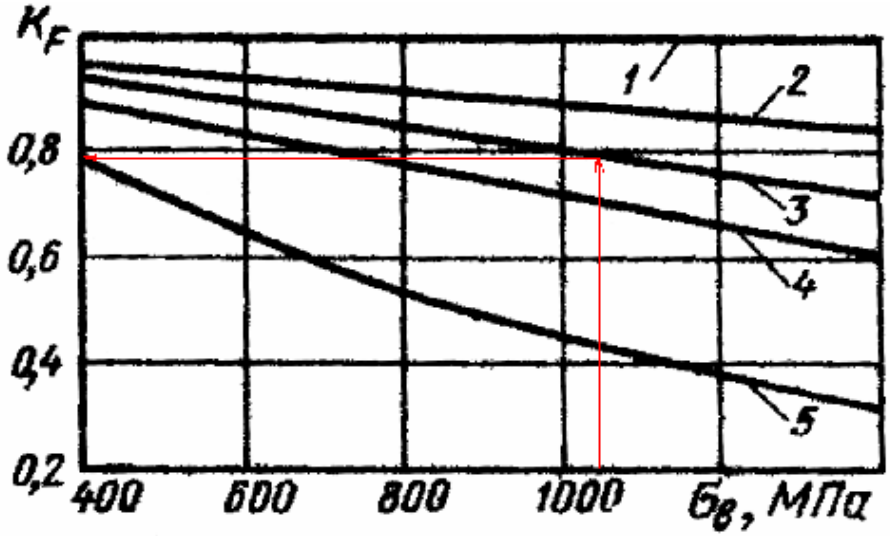

Fig. 28. Graph to determine coefficient quality processing surfaces :

					АЛ9412.06.00.00.00EN	Sheet
Ch.	Sheet	N document	Sign.	Date		

1 - processing surface using polishing , 2 - processing surface grinding m , 3 - processing surface with the help of fine turning , 4 - processing surface using the process of rough turning , 5 - scale is present on the surface .

Definition of effective the coefficient of concentration tensions with the help of formulas and (7) :

$$K_\sigma = 1 + (\alpha_\sigma - 1)\, q = 1 + (0.67 - 1)\, 0.4 = 0.868. \qquad (7a)$$

We choose coefficient impact $K_v = 1$. Using formula (6), we determine the value of the constructive coefficient

$$K_D = 1 /(0.868/1.02+1/0.8 - 1)/1 = 0.85. \qquad (6a)$$

Audit you look at the stress- strain state in the cladding elements with the help of the parameter y Nadai-Lode :

$$\chi_\sigma = 2 (\sigma_2 - \sigma_3) / (\sigma_1 - \sigma_3) - 1 \qquad (12)$$

From parameter assignment , creates a dependency to define tense state in and responds classified by type :

$\chi\sigma = -1$ – uniaxial stretching ; _ _

$\chi\sigma = 1$ – uniaxial e compression ; _

$\chi\sigma = 0$ – clean shift ;

$-1 < \chi\sigma < -0.5$ – stretching ;

$-0.5 < \chi\sigma < 0.5$ – displacement ;

$0.5 < \chi\sigma < 1$ – compression .

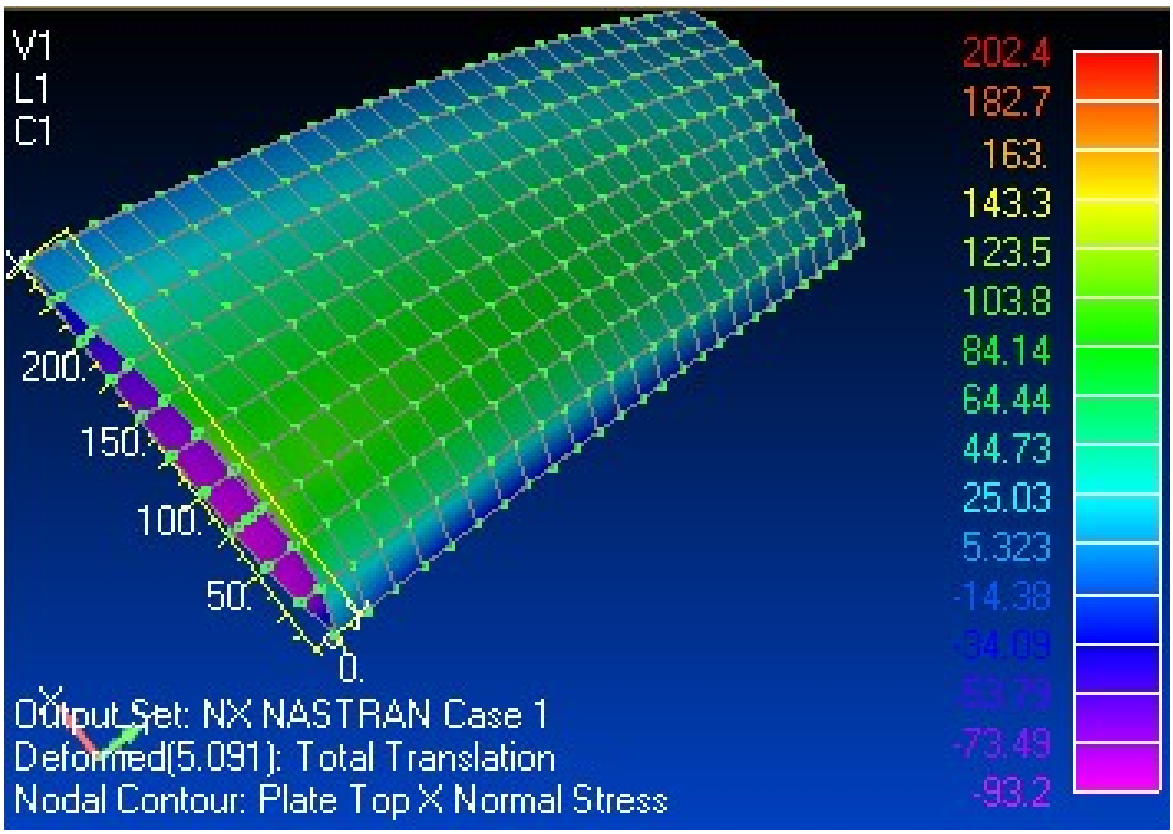

Fig. 29. Components of normal stresses in the cladding at $\sigma_1 = 123$ kgf/ sq.cm

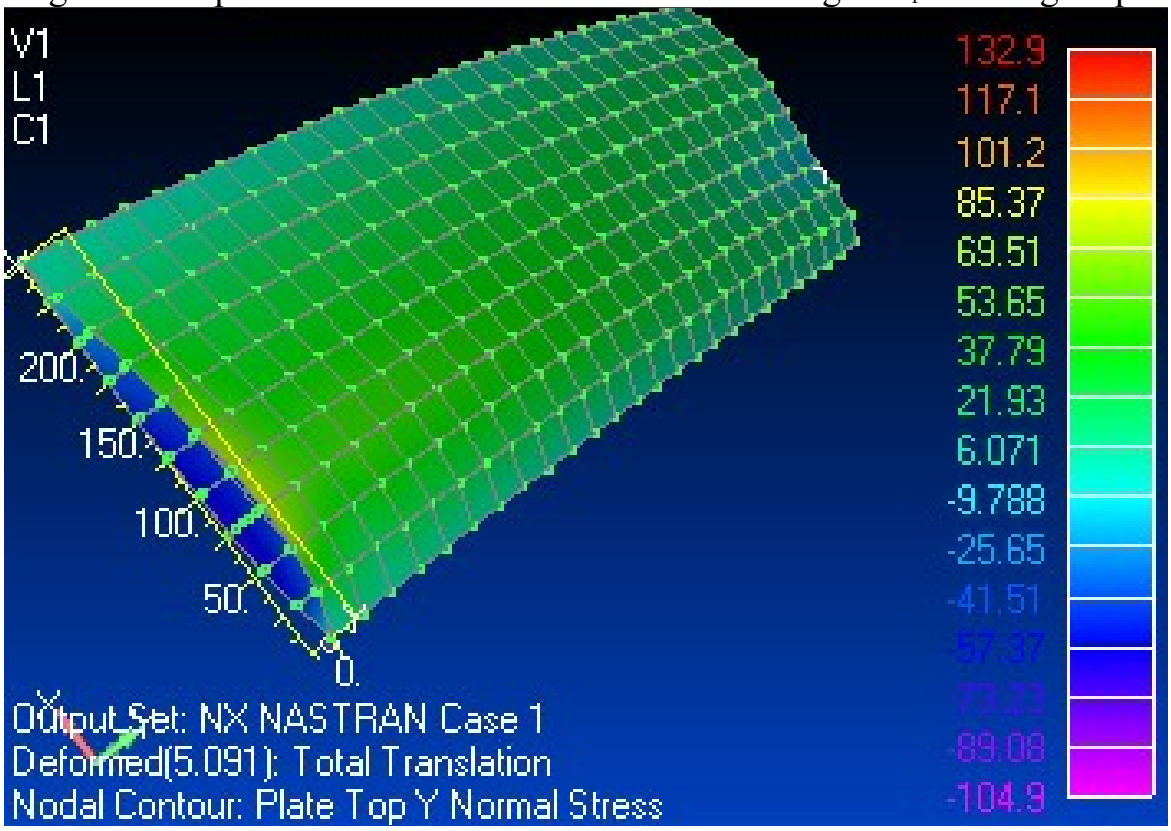

Fig. 30. Components of normal stresses in the cladding at $\sigma_2 = 69$ kgf/ sq.cm

$$\chi_\sigma = 2\,(\,69 - 0\,)/\,(123 - 0\,) - 1 \approx 0 \qquad (12a)$$

					AJI9412.06.00.00.00EN	Sheet
Ch.	Sheet	N document	Sign.	Date		

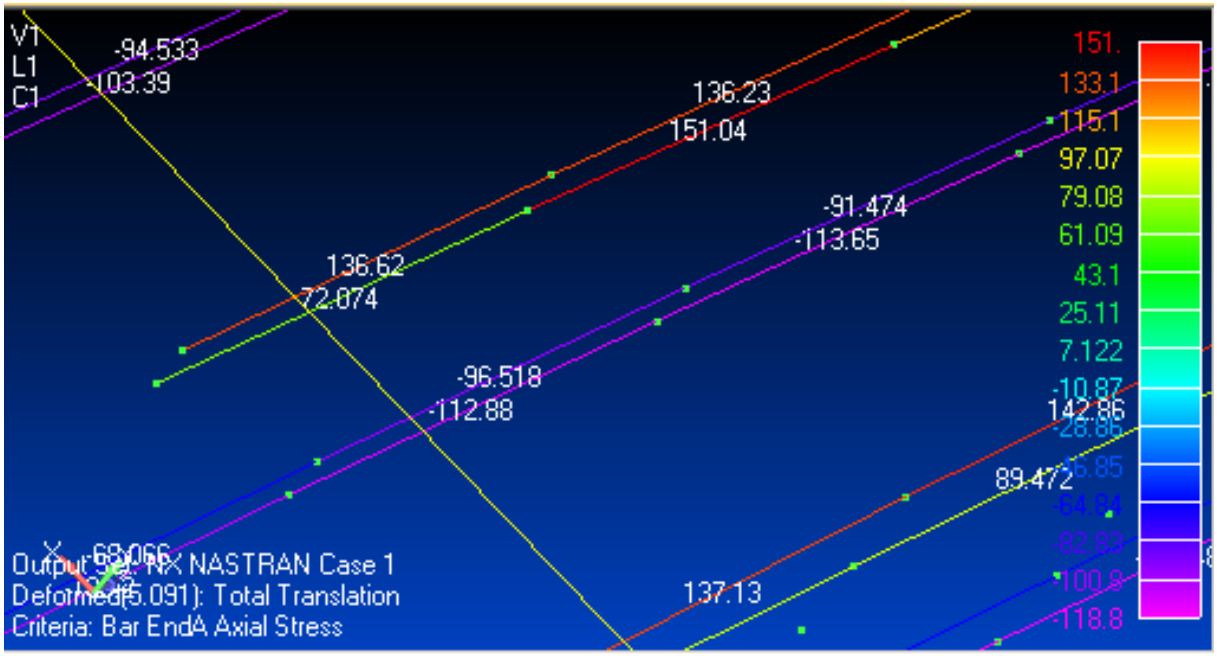

Fig. 31 . Axis normal tension two-node rods element iv at $\sigma_1 = 151$ kgf/ cm.sq

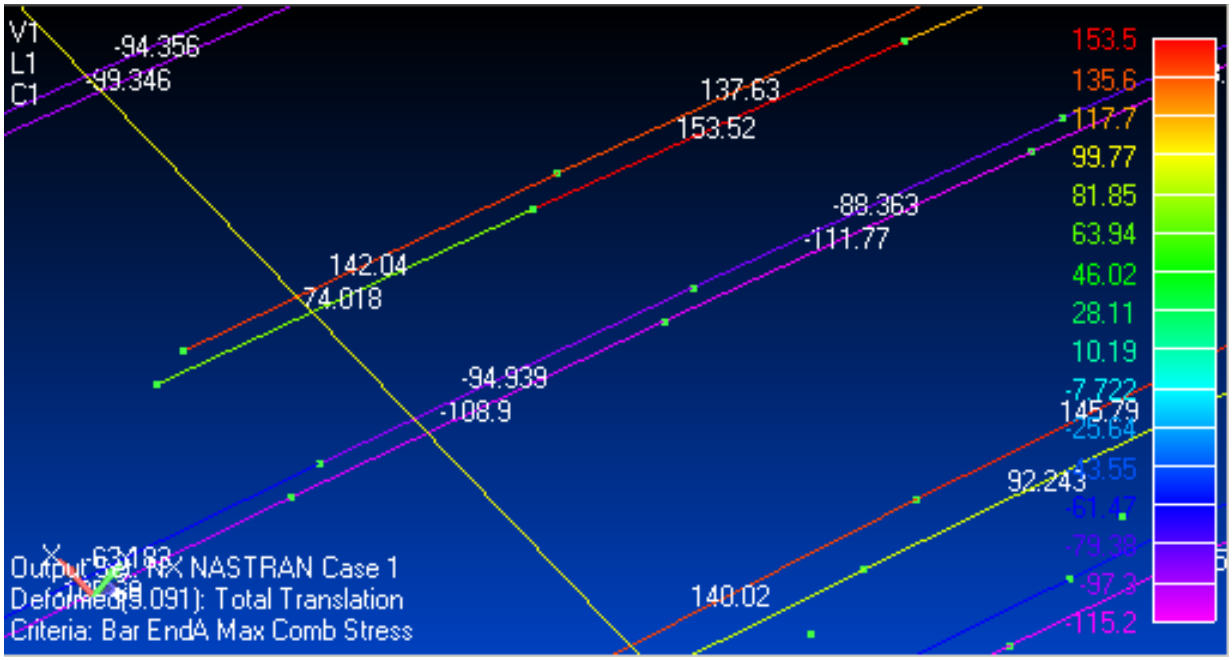

Fig. 32 . Maximum total tension in two-node elements at 153.5 kgf/ cm.sq

According to with formula (12) gives:

$$\chi_\sigma \approx 2(0 - 0) / (\sigma_1 - 0) - 1 = -1. \qquad (12, b)$$

The obtained stressed- strained state indicates the factor uniaxial stretching _

Endurance curve for aluminum 3 (Fig. 5.9).

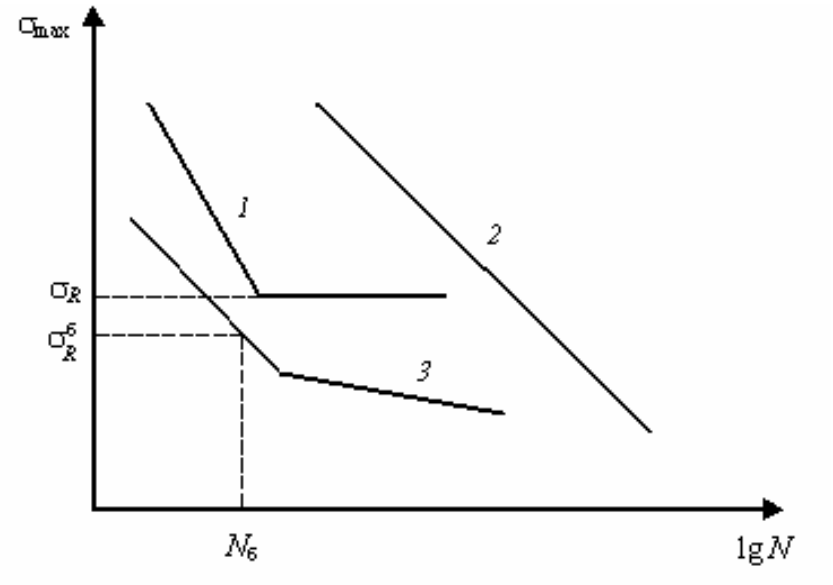

Fig. 33 . K riv a endurance Weller :
1 – low-carbon steel , 2 – high -strength steel , 3 – stainless steel and non-ferrous metals .

With the determined σ_D = 1845 kgf /cm ^{2} , taking into account the corresponding displacement of the curve along the OX axis, the number of cycles to failure during stretching -compression will be equal to Ns = 107.

Definition _ quantity and sections to the last limits of endurance

6 cycles take place in one hour for 1 minute and 10 oscillations . In total n = 60 oscillations per hour. General number cycles to the last limits of endurance Ns = 107 .

i_N = Nc / n ≈170,000 hours

number flights is equal to 17000 h. /4 hours = 40,000 flights .

ψ_1 = 10000 / 170000 = 0.058.

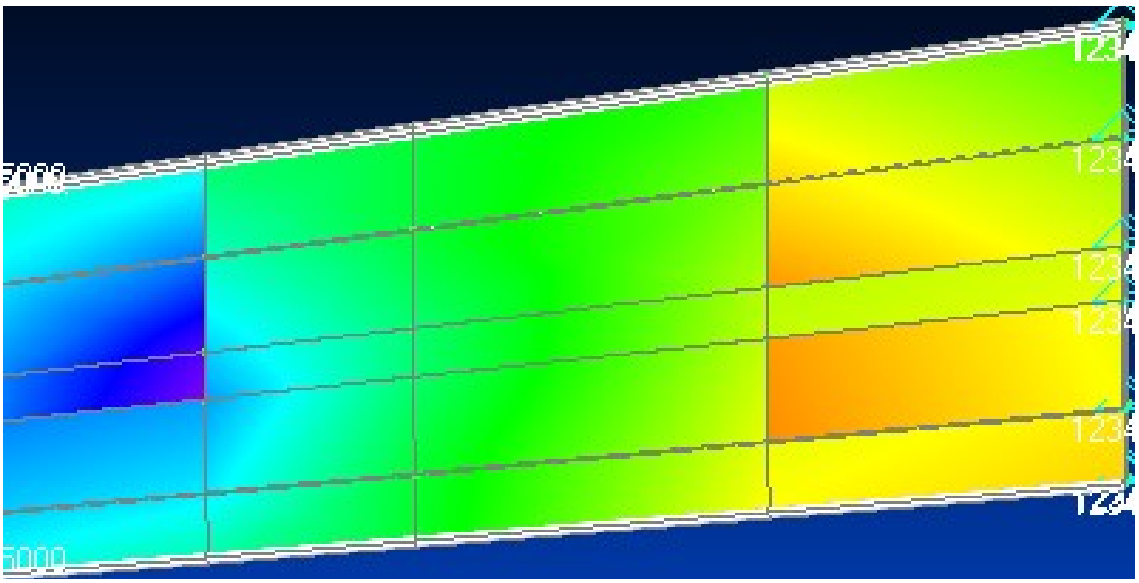

Fig. 34 . Section wings in plan

Let's calculate value torque from _ influence of lifting strength at a small angle and arrow-like χ

$$Mkr \approx (P/2) * (L/2) * \chi = 2000 * 8 * 0.15 = 2400 \text{ kgf /m.}$$

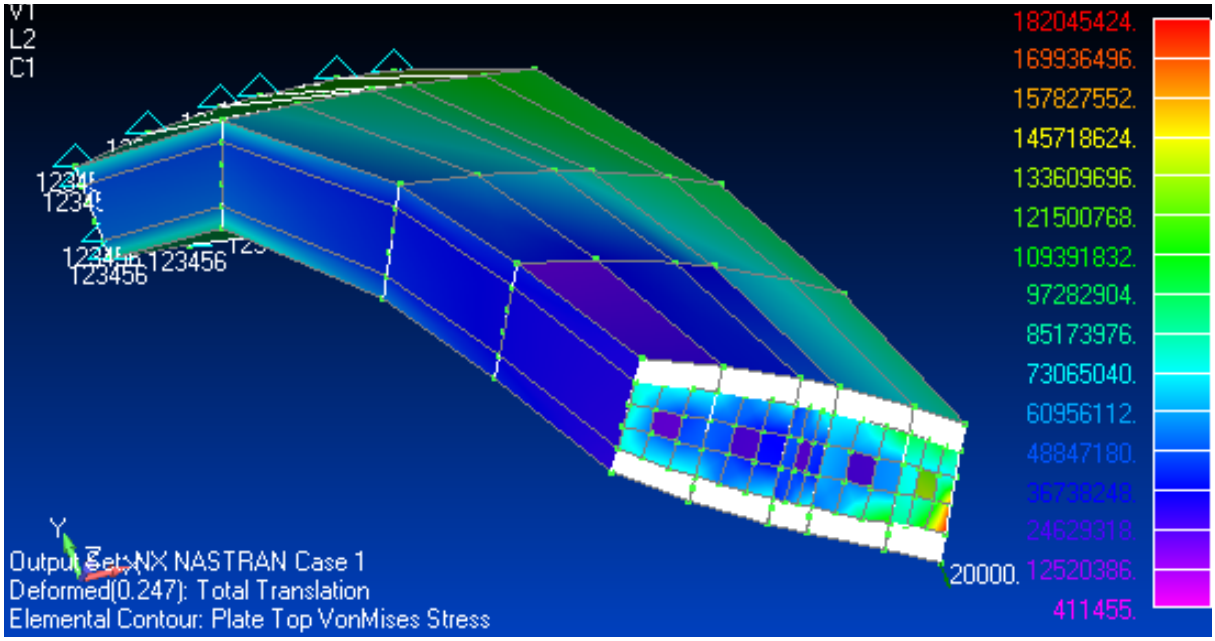

Fig. 35. Calculation of load on wings of LA during high angles of attack

Conclusions to the chapter

In this section were presented examples calculation of reflecting mechanism calculation endurance . were used in the calculations CAD and CAM systems . The used forecasting method, with the help of preliminary static calculation, simplifies the research and provides an accessible software module. For more accurate results calculation necessary use ati bigger number external factors and influence on the object in the process of systematization load.

Determination of aerodynamic characteristics of UAV

CAE systems are one of the most effective and fast methods of obtaining the results of mathematical calculations of an unmanned aircraft and analysis of models under investigation. CAE systems (Computer Aided Engineering) are used for automated work and study of analytical models that exist under certain conditions.

The purpose of this type of instrument is to provide flight data with unconditional compliance with all other limitations that exist in terms of controllability and flight safety, convenience, ease of operation, maintenance, etc.

The aerodynamic layout is practically reduced to the following tasks:

1) find the maximum values of the aerodynamic coefficient K and the lift coefficient, the smallest value of the frontal drag coefficient CXa with the most rational scheme of an unmanned aircraft and optimal wing parameters;

2) obtain smooth use of the disturbed stream. It is desirable that the failure occurs at the root of the wing and extends to its end;

3) to ensure the effectiveness of control returns in the entire range of angles of attack, including closed ones (welding, corkscrew);

4) elimination of harmful stagnant zones and eddy currents.

Use of the received data to construct LA polars

The curve that describes the dependence of the coefficient of frontal resistance Cx on the coefficient of lifting force Cy is called polar. Angles of attack and are also carried out on the curve.

For built polar aircraft, it is necessary to take into account the values of the coefficients Xx and Su, depending on the angles of attack. It is convenient to perform calculations in a table.

After filling in the table, you can start creating polars. To do this, points are plotted in the Cy and Cx coordinate system , which correspond to the angles of attack and are connected by a smooth curve.

The polar of an unmanned aircraft allows you to easily and quickly achieve a number of aerodynamic characteristics of the air, which are used in the calculation of flight characteristics.

An important characteristic that assessed the aerodynamic quality of the aircraft is the aerodynamic quality of K. increasing this indicator is one of the most important tasks of the aerodynamic layout of the aircraft.

The maximum aerodynamic quality of the unmanned aircraft will be achieved when shelling coal, using the points of contact of the line that passes through the time coordinates, keeping the tangent to the pole.

Description of application of CAE systems.

Solid Works 2020 system was chosen for data research, and the Flo Simulation package was additionally installed .

Solid Works 2007 system also used CAD systems at the stage of creating an analytical solid model of the aircraft. CAE Flo System Simula tion is specially used to model the processes used with the movement of liquid, air masses that interact with solid objects, taking into account the physical characteristics specified by the experimenter.

Trial

Parameters:

1. A solid CAD model provided by the CAE system

" Flo Simulation " of an unmanned aircraft;

2. Parameters of long words

test at a height of 1000 meters in the International

standard atmosphere;

- gaseous medium – used with a combination of environmental parameters " Air ";

- atmospheric pressure - 94,390 Pa;

- ambient temperature - 8.5 C °;

- Free forward speed

- flow capacity - 80 m/s;

- intensity of turbulence - 1%;

- turbulence length - 0.0205 m;

Test methods.

The test method is described in more detail.

Test results.

The tests made it possible to obtain the flight parameters required for testing the model.

During the tests, the results were obtained, which showed that the flow of air, which moves along the vertical axis, under the wing of an unmanned aircraft is from -4.2 to -1 m/s.

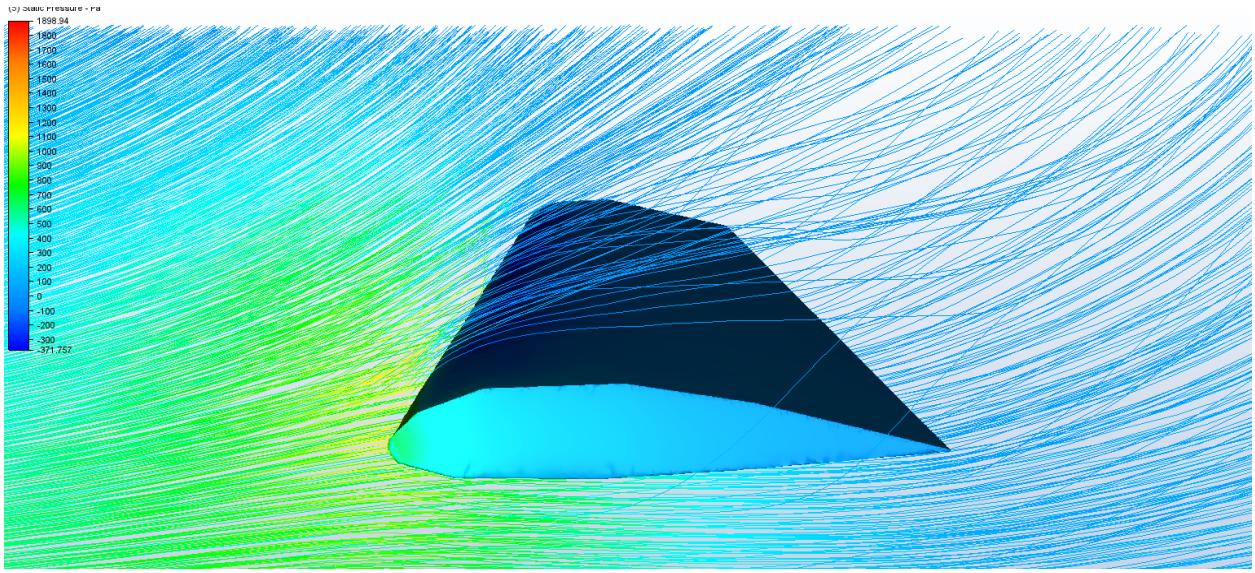

Fig. 36.

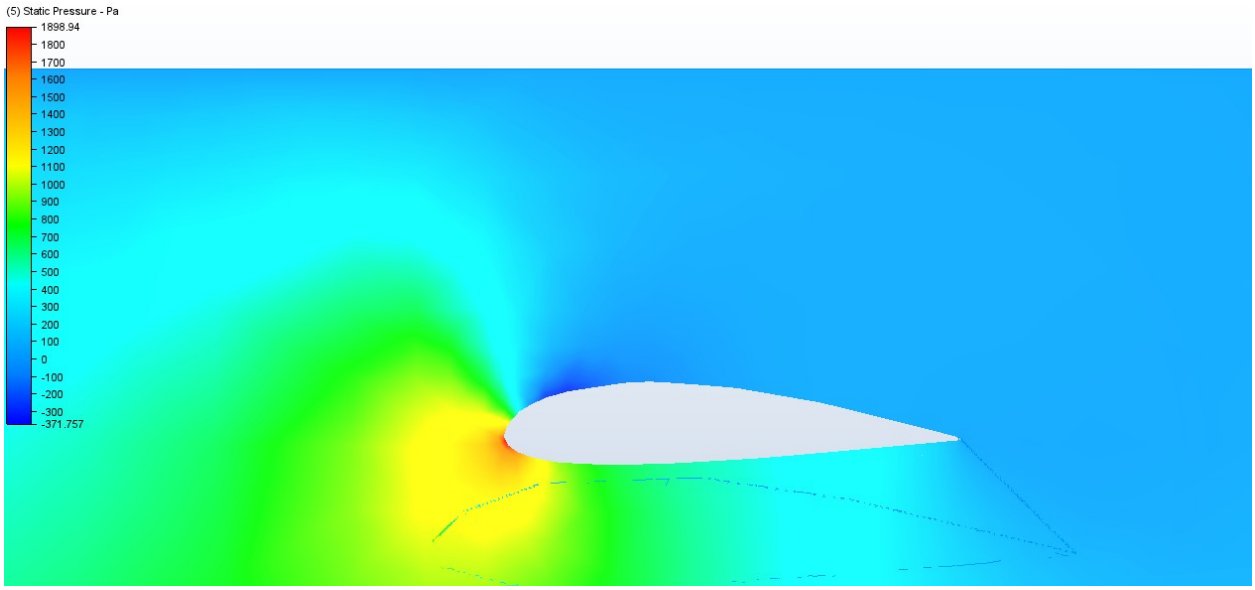

Fig. 37. Indicators of the speed of air flows along the vertical axis (m/s)
Aerodynamic calculations were carried out:

• Calculation and construction of dependence $C_{ya} = f(\alpha)$ for large numbers of M using means of mechanization and landing gear at zero height.

• Calculated and constructed polar $C_{ya} = f(C_{xa})$ for small numbers M for mechanization and chassis removed.

• Calculation and built cruise polar, not taking into account frontal drag.

• Calculation of the dependence of $C_y a = f(a)$ and the polarity of an unmanned aircraft for take-off, without taking into account the influence of the Earth.

Based on the obtained data, it was determined that the aircraft has good aerodynamic characteristics, which is confirmed by the visualization of aerodynamic loads in CDA systems.

Conclusion to the chapter

During the development of the project, basic aerodynamic calculations were performed, in particular, the calculated aerodynamic quality, which is equal to 18.304. External loads and strength calculations were also determined (for this, the model was simplified), as a result, it was determined that the largest displacements and stresses are observed in the area of attachment of the tail beam and vertical stabilizer. The following software was used to perform

this volume of calculations: Creo Parametric, Matlab, Autodesk_Simulation_CFD_2015.

7. Carbon Fibre Reinforced Polymer (CFRP) Composites.

The characteristics of composite materials are anisotropy, non-homogeneity and the fact that their reinforcing fibres are very abrasive; this make these materials more difficult to machine than metals (Abrate and Walton 1992). In modern manufactur- ing industries, common composite materials have different types of reinforcements and matrix compositions; in general they are divided into three major types: fibre reinforced polymers (FRP), metal matrix composites (MMC) and ceramic matrix composites (CMC). FRPs usually provide a higher specific strength and stiffness, and are lightweight compared to traditional steels. These characteristics make FRPs the favoured material for high performance applications, such as in Formula-1 cars and combat aircraft components, despite the fact that they are expensive to manufacture (Komanduri 1997). The strength of FRPs is relatively low when they reach their maximum-use temperature, because this type of material is prone to chemical decomposition or degradation at even moderate temperatures. For exam- ple, carbon fibres can endure temperatures of up to 3000 °C until degradation of the structure is initiated (Pecat et al. 2012). MMCs are suitable for higher operating temperature applications compared to FRPs. Continuous fibres in MMC provide the highest stiffness and strength, whereas other types such discontinuous and particu- late fibres have better dimensional stability compared to unreinforced alloys, which Fig. 38 shows specific strength versus specific stiffness for various MMC materials and each composite indicates the number for the reinforcement volume fraction. The main performance of using CMC is to improve fracture toughness during appli- cations. For heavy cuts, or to avoid fracture during cutting, CMCs exhibit an increased toughness compared to ceramic cutting tools. CMCs are superior to met- als due to higher specific modulus and

mechanical properties at elevated tempera- tures. In many types of composites, FRPs count among the most high-performance materials in the field of light-weight design (Pecat et al. 2012). Aircraft and aero- space design in particular has benefitted from carbon-fibre-reinforced polymers (CFRPs), which today are the most popular composite in the aerospace industry (Caggiano et al. 2018, Brouwer 2019, Dandekar and Shin 2012, Garrick 2007, Askeland and Phulé 2006, Komanduri 1997, Santhanakrishnan et al. 1988).

Composites are categorized into two main groups, depending on the way the fibres are arranged within the matrix. Figure 2.3 shows the schematic illustration of reinforcing plastics; the first group is called fibre-reinforced composites, whereas the second group is called particle-reinforced composites. Each group of compos- ites has a different reinforcement mechanism and strengths, depending on the appli- cation. FRPs consist of fibres (in discontinuous or dispersed phase) in a plastic matrix (the continuous phase) (Kalpakjian and Schmid 1999). In components man- ufactured from long - or even continuous - fibre reinforced composites, such as unidirectional or cross-ply laminates, anisotropy may be desirable as it can be arranged so that the maximum service stress lies in the direction that has the highest strength (Matthew and Rawlings 1999).

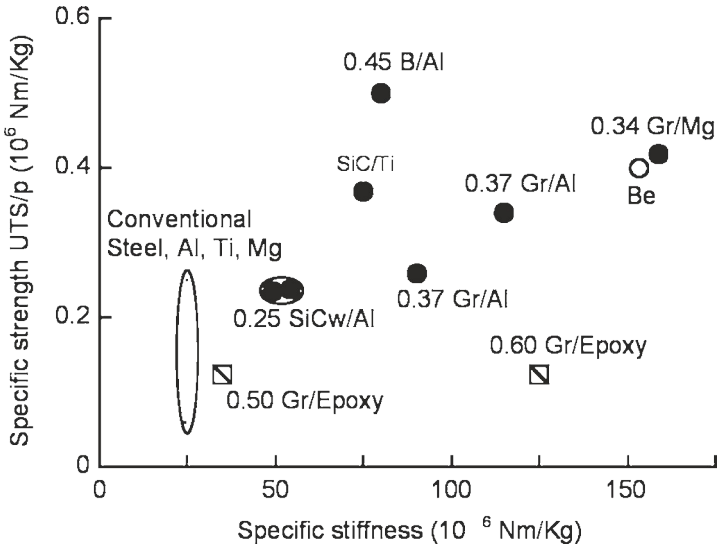

Fig. 38. Specific strength versus specific stiffness for various MMC materials (adapted from Teti 2002)

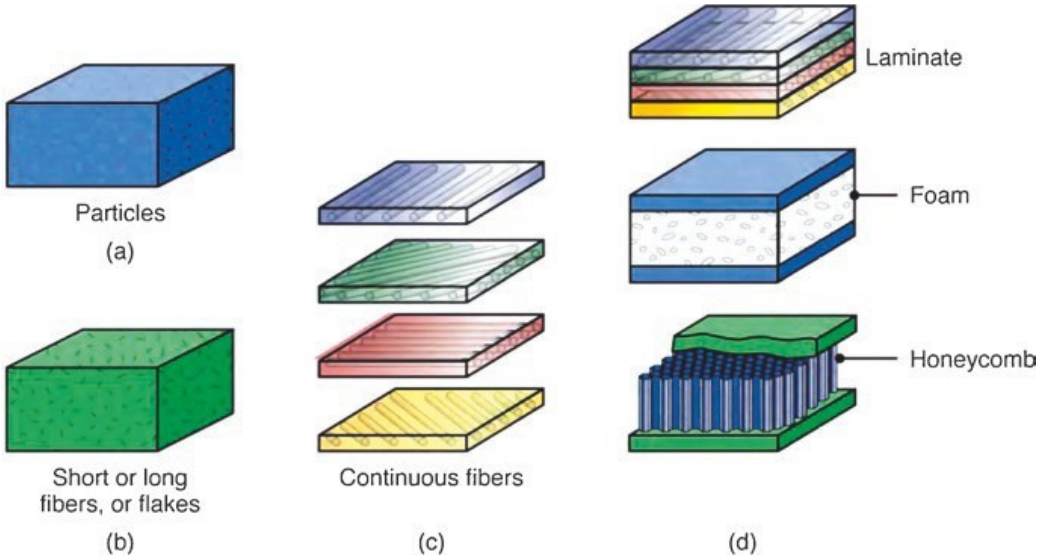

Fig. 39. Schematic illustration of methods of reinforcing plastics (matrix) with (a) particles; (b) short or long fibres or flakes; and (c) continuous fibres.

The laminate structures in (d) can be manufactured from the layers of continuous fibres or sandwich structures using a foam or honeycomb core (Kalpakjian and Schmid 2016). However, unidirectional orientations pro- vide poor properties if the load is perpendicular to the fibres (Askeland and Phulé 2006). Most fibre-reinforced composites provide improved strength, fatigue resis- tance, Young's modulus, and strength-to-weight ratio, by incorporating strong and stiff but brittle fibres into a softer, more ductile matrix (Askeland and Phulé 2006). Boron, carbon, polymers (aramids) and ceramics provide exceptional reinforcement in advanced composites, based on matrices of polymers, metals, ceramics and even intermetallic compounds (Askeland and Phulé 2006, Matthew and Rawlings 1999). Epoxies comprise 80% of the matrix materials used in reinforced plastics, but poly- esters are also used as they are less expensive (Kalpakjian and Schmid 1999). Moreover, as Askeland and Phulé (2006) pointed out, several directions of the matrix can be arranged in long continuous fibres; for example, orthogonal arrange- ments with 0°/90°

plies which have good strength in two perpendicular directions. More complicated arrangements such as 0°/±45°/90° plies provide reinforcement in multiple directions. Figure 40 shows the different fibre orientation and fibre arrangement types. The most common types of FRPs are Aramid-Fibre Reinforced Plastics (ARFP), Glass-Fibre Reinforced Plastics (GFRP), Carbon-Fibre Reinforced Plastics (CFRP).In addition, another type of FRP composite called Kevlar-Fibre Reinforced Plastics (KFRP) initially introduced by du Pont in 1972 under the trade name Kevlar® and this type of composite is also categorised under Aramid fibres (Komanduri 1997). These three composites are very similar in their fabrication pro- cess, but each composite has a different machining behaviour due to its difference in physical and mechanical properties (Santhanakrishnan et al. 1988)

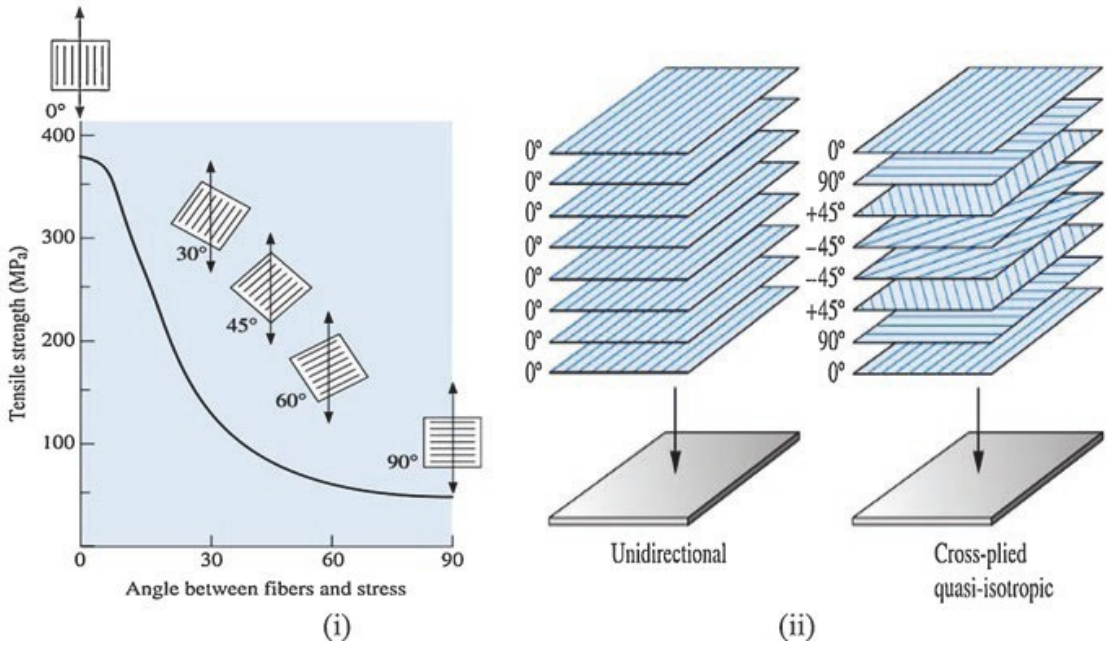

Fig. 40 (**i**) Effect of fibre orientation on the tensile strength of E-glass fibre-reinforced epoxy composites; (**ii**) Several directions within the matrix for long, continuous fibres) (Askeland and Phulé 2006)

Good surface finish and integrity, long tool life, and low force and power require- ments are important elements of good machinability (Kalpakjian and Schmid 1999). Drilling produces holes for mechanical joints such as rivets,

bolts and screws, which it is one of the most frequent operations in manufacturing. Only an appropriate tool geometry using the correct process conditions, and ideal machin- ing performance, will produce a level of damage that is acceptable (Reza 2010). In the case of components made from carbon fibre-reinforced polymers, it is often necessary to machine the components - for example to make holes or trim the edge - but the cutting of CFRPs is often associated with delamination of the com- posites and short tool life (Koplev et al. 1983). The machinability of composites depends on the fibre type, fibre volume content, fibre orientation, and the manufac- turing process. It is difficult to analogize the surface formation and tool wear mechanisms seen in the machining of composites from the data obtained in the cutting of homogenous material such as steel (Pecat et al. 2012, Santhanakrishnan et al. 1988, Komanduri 1997). Furthermore, as Pecat et al. (2012) postulated, due to non-

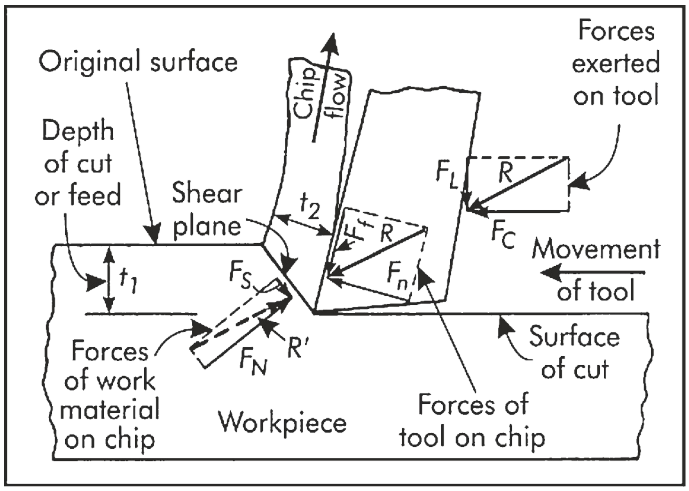

R: the tool exerts a force
F_n: a normal component on chip
F_f: a friction component
R: equal and opposite reaction from the workpiece at the shear plane
Fs: shearing force along the shear plane
Fc: a component in the direction of tool movement
F_N: forces of work material on chip
T_1: undeformed chip
T_2: deformed chip
F_L: a normal component on tool

homogenous and anisotropic material properties, machining of CFRP pres- ents specific difficulties like fibre pull-out, delamination and decomposition of matrix material, which leads to a degradation of surface quality and material properties.

Fig. 41 Forces exerted by cutting tool – orthogonal cutting (Schrader and Elshennawy 2000)

Three components as shown in Fig. 42(d). The first one is Fc which is a primary cut- ting force acting in the direction of the cutting velocity vector; it is

the largest force geometry and accounts for 99% of the power required by the process. Next is Ff, which is a feed force acting in the direction of the tool used; it is usually about 50% of Fc, but it accounts for only a small percentage of the power required, because feed rates are usually small compared to cutting speeds. Finally, Fr is the radial or thrust force acting perpendicular to the machined surface; typically Ff contributes very little to the power requirements, because velocity in the radial direction is negligi- ble. The main benefit of oblique cutting is that it is a means of controlling chip flow. There are three most common types of chips (Askeland and Phulé 2006, Schrader and Elshennawy 2000, Kalpakjian and Schmid 1999)..

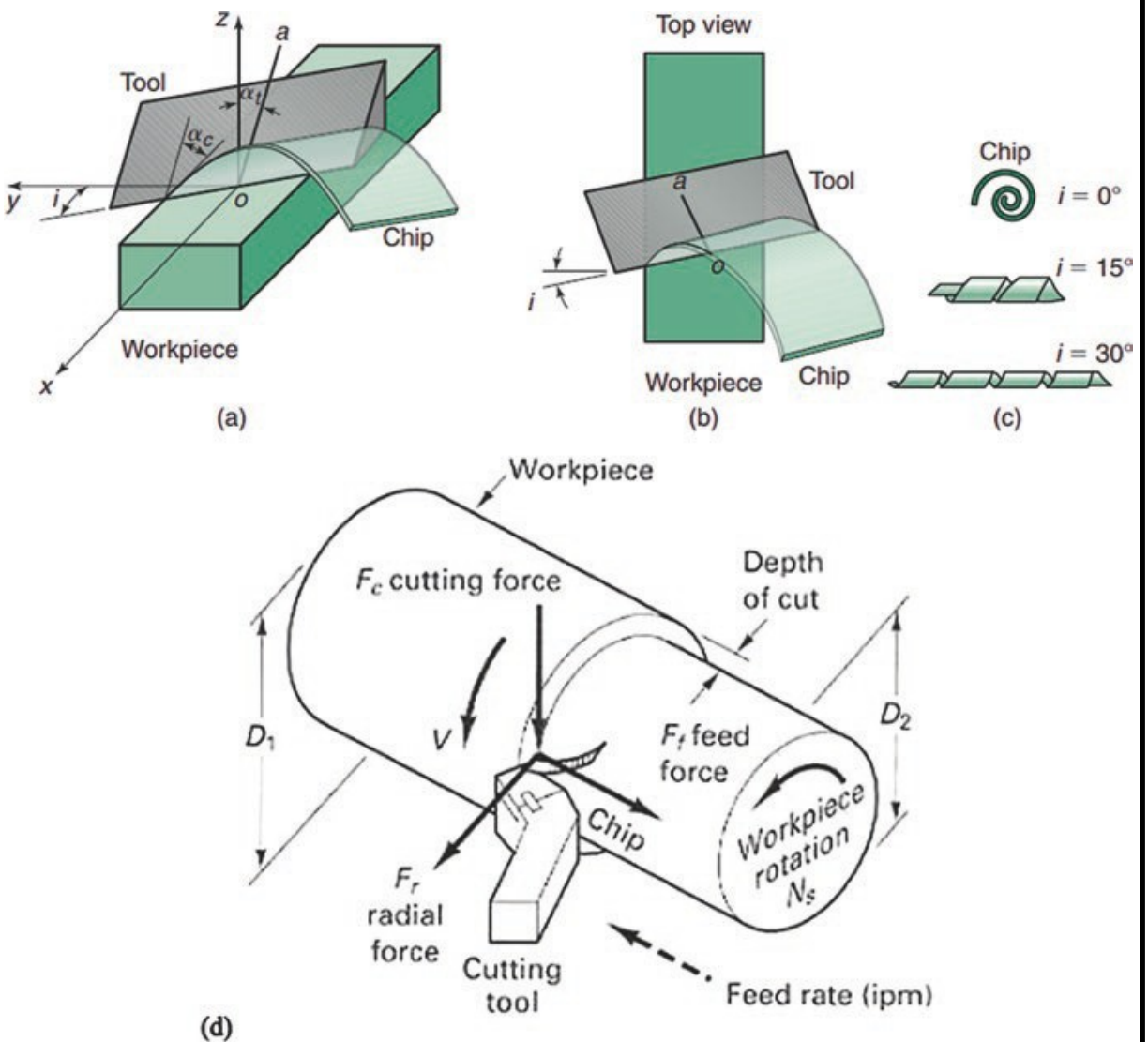

Fig. 42. (a) Schematic illustration of oblique cutting; (b) Inclination angle showing at the top view; (c) Types of chips being produced by different inclination; and (d) Oblique machining has three measurable components of forces (Kalpakjian and Schmid 1999)

The first type are called con- tinuous chips; the conditions that favour their production are small chip thickness, high cutting speed, sharp cutting edge, large rake angle in cutting tool and fine feed, smooth tool face and efficient lubricating system. Such chips are produced while machining ductile materials like mild steel, copper and aluminium

Due to the plas- tic deformation of ductile material, long and continuous chips are produced; this is desirable because it produces good surface finish, low power consumption and lon- ger tool life. These chips are difficult to handle and dispose of, furthermore they coil in a helix, and curl around the workpiece and tool. The tool face is in contact for a longer period, resulting in more frictional heat; however this problem could be recti- fied by the use of chip breakers, clamped onto the rake face of the cutting tool. During machining, long and continuous chips will affect machining. The chips should be broken into small pieces for easy removal, safety and to prevent damage to the machine tool and workpiece. The function of chip breakers is to reduce the radius of curvature of chips and thus break them. The upper side of continuous chips is notched, while the lower side which slides over the face tool is smooth and shiny. The chips have the same thickness throughout. The second type of chips are called discontinuous; these chips are produced when cutting more brittle materials like bronze, hard brass and gray cast iron. Since the chips break up into small seg- ments, the friction between chip and tool reduces, resulting in a better surface finish. The smaller chip segments are more convenient to handle and dispose of. Discontinuous chips are also produced in ductile materials under conditions such as large chip thickness, low cutting speed, or small rake angle of tool. Brittle materials lack the ductility necessary for appreciable plastic chip

deformation. The amount of deformation which the chip undergoes is limited by repeated fracturing. If these chips are produced from brittle materials, then the surface finish is fair, power con- sumption is low and tool life is reasonable; however, with ductile materials the surface finish is poor and tool wear is excessive.

Chips with built-up edges are the final type. The edges are simply small built-up areas sticking to the nose of the cutting tool, which occur with continuous chips (Schrader and Elshennawy 2000). When machining ductile materials, due to condi- tions of high local temperature and extreme pressure of the cutting zone, and also high friction in the tool chip interface, the possibility exists for the workpiece mate- rial to weld to the cutting edge of the tool, thus forming built-up edges. This weld metal is extremely hard and brittle, and the welding may affect the cutting action of the tool. Successive layers are added to the built-up edge; when it becomes large and unstable, it is broken and part of it is carried up the face of the tool along with chip, while the remainder is left in the surface being machined, contributing to the rough- ness of the surface. The size of the built-up edge varies during the machining opera- tion - it increases, then decrease and again increases. This built-up edge protects the cutting edge of the tool, thus changing the geometry of the cutting tool. Low cutting speeds lead to the formation of a built-up edge, however, with the higher cutting speeds associated with sintered carbide tools, the built-up edge is negligible or does not exist. Conditions favouring the formation of built-up edges are low cutting speed, low rake angle, high feed and large depth of cut. This formation can be avoided by the use of coolants and taking light cuts at high speeds, which in turn leads to the formation of a crater on the surface of the tool.

Conclusions to the chapter.

Carbon-based composite materials have advantages specifically for jet-powered aircraft. They provide the necessary strength, heat resistance and aerodynamic quality of the surface of the UAV. The technology that will allow the production of a high-quality UAV glider is considered.

GENERAL CONCLUSIONS

In the course of this work, an unmanned aerial vehicle with a "duck" aerodynamic scheme with a jet engine was developed. It has a mixed construction (metal frame, wing and tail, fiberglass fuselage), each unit is designed to perform its functions in the best possible way with minimal weight and the required strength and endurance. An aerodynamic calculation was carried out, and the main aerodynamic characteristics were also determined. Aerodynamic characteristics were calculated, including a flight range of 4,000 km and a flight time of 4.5 hours, which significantly increases the capabilities of such UAVs.

External loads and strength calculations were also determined, as a result of which it was determined that the largest displacements and stresses are observed in the area of attachment of the tail beam and vertical stabilizer. On the basis of the obtained results, the optimization of this design was carried out, and recommendations were made to improve the aerodynamics of this model. The optimal design of the UAV has been developed according to the indicators of useful weight - range - speed. A model of the power structure was developed, aerodynamic loads were checked, and optimization of this structure was performed based on the obtained research.

The work used such research methods as: three-dimensional modeling in CAD CAM systems, finite element method, information and communication technologies, mathematical modeling. The results of this work show ways to optimize and improve this design, in the future, they will help future engineers with the justification of this type of design as part of the development of a promising UAV project.

Nowadays, composite materials are increasingly in demand, they are steadily replacing their predecessors. Due to their versatility, it was decided to use composite materials in the design of the aircraft.

REFERENCES

1. SkyShips YourTube Channel [Electronic resource] Access mode: https://www.youtube.com/c/SkyShips
2. Cessna Citation Mustang [Electronic resource] Access mode: https://www.lunajets.com/ru/flot/cessna/citation-mustang
3. Cessna Citation Mustang [Electronic resource] Access mode: https://www.the-blueprints.com/vectordrawings/show/1933/cessna_citation_mustang/
4. Honda HA-420 HondaJet [Electronic resource] Access mode: https://www.the-blueprints.com/vectordrawings/show/4718/honda_ha-420_hondajet/
5. Cessna Citation Mustang [Electronic resource] Access mode: https://uk.wikipedia.org/wiki/Cessna_Citation_Mustang
6. Embraer Phenom 100 [Electronic resource] Access mode: https://en.wikipedia.org/wiki/Embraer_Phenom_100
7. Honda HA-420 HondaJet [Electronic resource] Access mode: https://en.wikipedia.org/wiki/Honda_HA-420_HondaJet
8. [Electronic resource] Access mode: https :// studbooks . net /2447681/ tehnika / solidworks _2014
9. Mkhitaryan A.M. etc. Flight dynamics. - M.: Mashinobuduvaniya, 1978. - 422 p.
10. Ligam T.I. Aerodynamics and flight dynamics of turbojet aircraft. - Moscow: Transport, 1979. - 319 p.
11. Romasevich V.F., Samoilov G.A. Practical aerodynamics of helicopters. Moscow: Transport, 1972. - 184 p.
12. Composite Materials: Applications in Engineering, Biomedicine and Food Science [Electronic resource] Access mode: https://ebin.pub/composite-materials-applications-in-engineering-biomedicine-and-food-science-1st-ed-9783030454883-9783030454890.html